

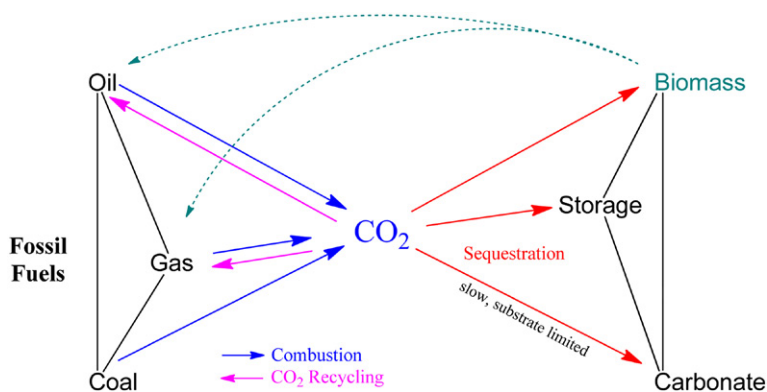
Biomimetic Approaches to Reversible CO₂ Capture from Air. *N*-Methylcarbaminic Acid Formation in Rubisco-Inspired Models

*Rainer Glaser, Paula O. Castello-Blindt,
and Jian Yin*

Department of Chemistry, University of Missouri, Columbia, MO 65211, USA

17.1 INTRODUCTION

Carbon tracking in the atmosphere started more than 50 years ago with continuous CO₂ measurement at Mauna Loa and resulted in the iconic “Keeling Curve,” the first demonstration of the seasonal variations of CO₂ concentrations and the steady rise of the annual average CO₂ concentration [1,2]. Carbon tracking has since been expanded systematically and NOAA’s modern data assimilation system “CarbonTracker” [3] employs a set of 28,000 CO₂ mole fraction observations in the global atmosphere (surface, towers, small aircraft) to study the CO₂ exchange between the biosphere and the atmosphere as a function of time [4]. Strategies to obtain better carbon inventories have been under development by the US Carbon Cycle Science Program [5–7] and NASA has been planning global space-based CO₂ observation (i.e., Orbiting Carbon Observatory, OCO-2 [8]). While considerable uncertainties remain with regard to accounting for all CO₂, all reports on carbon inventories consistently show that carbon sources far outweigh carbon sinks: the global atmospheric CO₂ concentrations have been growing steadily and at Mauna Loa the average annual mean increased from 316.0 ppm in 1959 to its current value of 394.3 ppm in 2012 [2] (see [Scheme 17.1](#).)



SCHEME 17.1 Global emissions of carbon to the atmosphere amounted to 9.5 ± 0.5 PgC in 2011 (34.7 billion tonnes of CO₂) and total emissions are growing annually by about 1.4%.

The Intergovernmental Panel on Climate Change (IPCC [9]) reported in its fourth assessment report in 2007 (AR4 [10]) an average rate of increase in CO₂ of 1.4 ppm yr^{-1} based on direct instrumental measurements over the period 1960–2005 and projected a worst-case estimate of 2.3% growth (rapid economic growth, globalization, intensive fossil fuel use). The Earth Policy Institute [11] reported total carbon emissions of 7.980 PgC (petagram of carbon, 10^{15} g carbon) in 2008 and projected a rise to 9.927 PgC by 2020 assuming an average increase of emissions by 1.4%. The Global Carbon Project [12] reported in its “Carbon Budget 2012” [13] an estimated total emission of 9.5 ± 0.5 PgC to the atmosphere in 2011.

While the overwhelming majority in the earth sciences community agrees that the environmental problems caused by greenhouse gases are of a magnitude that is simply unimaginable, the communication of the urgency of addressing the CO₂ problem has met with enormous obstacles [14,15]. The history and collapse of the Kyoto protocol and the fierce resistance to IPPC are well documented [16]. There seems to be a consensus that atmospheric CO₂ stabilization will require a portfolio of solutions including increases in energy efficiency, the development of renewable energy production, and the large-scale deployment carbon capture and storage (CCS) systems [17–21].

Technologies for carbon capture and storage mainly have focused on CO₂ capture at concentrated sources. One way to remove CO₂ from the exhaust of a combustion plant involves exhaust cooling to condense liquid CO₂. The cooling may involve several stages of productive heat exchange and only the final refrigeration is an energy-consuming process. Ammonia absorption refrigeration for CO₂ capture at a rate 2.7 kg/s liquid CO₂ has been demonstrated for a 25 MW plant [22]. In its ECO₂ process, Powerspan [23] uses an ammonia solution (NH₄OH) for post-combustion CO₂ capture from the flue gas (as NH₄HCO₃). The captured CO₂ is then released in a form that is ready for further compression to liquid CO₂. Alstom [24] has been developing a similar process that employs a chilled ammonia solution [25] to capture CO₂ from flue gas as ammonium bicarbonate. Various ethanolamines are under investigation as alternatives to ammonia that can be used in higher concentration and at higher temperatures [26] and these include monoethanolamine (MEA), diethanolamine (DEA), and

methyldiethanolamine (MDEA). MEA shows particular promise [27] and MEA/MDEA mixtures also have been employed with success [28].

In 2004, Zeman and Lackner discussed CO₂ capture from air as the method of last resort to combat excessive atmospheric CO₂ concentrations [29,30]. CO₂ scrubbing involves the capture of CO₂ from air by a substrate, the release of CO₂ from the substrate and its collection, and the long-term CO₂ sequestration. Global Research Technologies (GRT) first demonstrated CO₂ capture from air with their ACCESS™ system in 2007 [31]. The device consisted of 32 hanging, 3.2 m² panels of proprietary plastic which adsorb CO₂ at a rate of 23 kg per day. To capture all the emissions, GRT envisioned the deployment of 20 million, shipping container-sized devices around the globe [32]. GRT's main targets for possible commercial uses of captured CO₂ are controlled environment agriculture (CEA greenhouses) and algae cultivation (biofuel feedstock). Such markets already exist and greenhouse farmers pay up to 300 dollars/ton of CO₂. In their 2006 article, Keith, Ha-Duong, and Stolaroff reported on their assessment of the ultimate physical limits on the amount of energy and land required for air capture [33]. These authors describe two systems that might achieve air capture using current technology and do so at a cost of less than 200 and 500 dollar/ton of carbon, respectively. In its report in 2011, a committee of the American Physical Society (APS) reviewed CCS technologies and estimated the cost of direct air capture with chemicals at about \$600/ton of CO₂. The APS committee pointed out that CO₂ capture from the air would only make economic sense after the more cost-effective CO₂ capture from concentrated sources (i.e., coal plant smokestack) were fully implemented and CO₂ capture from the air would then present the pertinent tool to address CO₂ emissions from distributed sources [34,35].

All methods for CO₂ capture at concentrated sources or from air rely on a chemical system for reversible CO₂ capture. There has been a rapid development of amines (*vide supra*), of polyamine-based regenerable solid adsorbents [36], and of alkylamine-appended metal-organic framework [37–39]. Alternatives to amine-based capture systems also have been explored and these include, for example, polyethylene glycol promoted CO₂ chemistry [40]. The success of any CO₂ capture system relies on the thermochemistry and the kinetics of the CO₂ capture reaction. The thermochemistry of the CO₂ capture reaction must ensure the effective capture as well as the possibility for the subsequent CO₂ release. The kinetics of the CO₂ capture reaction must be such that both the capture and the release of CO₂ are not hindered too much by the activation barriers. Biomimetic CO₂ capture systems are of special interest because they hold promise to meet both the thermodynamic and the kinetic requirements for reversible CO₂ capture. For example, the bio-CO₂ capture in carbonic anhydrase II from *Chlorella vulgaris* has been characterized [41].

We have been interested in the properties of heterocumulenes [42–44] and we have studied nucleophilic addition chemistry of CO₂ [45] and carbodiimide [46,47]. In this context, we are developing rubisco-based biomimetic systems for reversible CO₂ capture from air. In this chapter, we review the mechanism of rubisco-based biological CO₂ fixation, we identify the carbamoylation reaction of the activator CO₂ in the active site of rubisco as a candidate for the development of a chemical CO₂ capture and release system, we discuss the construction of several models and describe the equations for the thermochemical assessment, and we present the results of computational studies of the small molecule model systems to explore the thermochemistry of the carbamoylation reaction.

17.2 BIOLOGICAL CO₂ FIXATION AND BIOMIMETIC APPROACHES TO CO₂ SCRUBBING

17.2.1 Rubisco-Catalyzed Biological CO₂ Fixation

Rubisco (ribulose 1,5-bisphosphate carboxylase/oxygenase, a.k.a. RuBisCO) catalyzes the addition of CO₂ and water to RuBP (D-ribulose 1,5-bisphosphate) in the photosynthetic carbon assimilation via the Calvin-Bassham-Benson cycle and results in two molecules of 3-PGA (3-phospho-D-glycerate) and 0.5 O₂ [48–50]. The carboxylation reaction competes with photorespiration, that is, the fixing of molecular O₂ by addition of O₂ to RuBP to form one equivalent of 3-PGA and one equivalent of phosphoglycolate. This competition necessitates the photorespiratory pathway to recycle the 2-phosphoglycolate to RuBP and the release of CO₂ (one CO₂ for every two molecules of fixed O₂). Nearly all carbohydrate production in the biosphere (ca. 10¹⁴ kg CO₂ per year, or 27.3 PgC yr⁻¹) depends on rubisco catalysis and rubisco is the most abundant protein on Earth. Rubisco does have a much higher affinity for CO₂ ($K_m = 9 \mu\text{M}$) than for O₂ ($K_m = 535 \mu\text{M}$), but nevertheless the photosynthetic yield is limited by the oxygenase reaction because of the small [CO₂]/[O₂] ratio in the atmosphere.

Many photosynthetic organisms contain form I rubisco [51] which is comprised of eight large (L) and eight small (S) subunits and the crystal structure of spinach *Spinacia oleracea* [52] provided an early example of such a hexadecameric rubisco [53]. Form II rubisco lacks small subunits, generally occurs as L₂, has very low S_{c/o} values and higher turnover numbers, and form II is exemplified by the bacterial rubisco of *Rhodospirillum rubrum* [54]. An example of an L₂S₂ rubisco occurs in the crystal structure of activated rice rubisco complexed with the reaction intermediate analog 2-carboxyarabinitol-1,5-bisphosphate [55]. We focus on form I rubisco and this form also occurs in algae and prominent examples include the green algae *Chlamydomonas reinhardtii* [56] and the red algae *Galdieria sulphuraria* [57]. Each L₈S₈ unit contains four L₂ dimers and two S₄ tetramers, features a non-crystallographic fourfold axis with a central channel, and the S-subunits control the size of the entrance channel. The C-terminal extension of the S-subunit lies on the protein surface anchored by interactions with the N-terminal region of the S-subunit. Changes in the position of this N-terminus affect the conformation of rubisco and its diphosphate binding ability [58], and this feature may play a major role in rubisco activation.

Hartmann and Harpel [59a] and Lorimer et al. [59b] discussed the mechanism of rubisco catalysis. To exhibit both the carboxylase and oxygenase activities, rubisco must be activated through the carbamylation of active-site lysine (Lys) by an activator CO₂ (^ACO₂). The carbamate thus formed is stabilized both by complexation to Mg²⁺ and by NH...OC hydrogen-bonding (Scheme 17.3 and Figure 17.1). It is an idiosyncrasy of rubisco that the other substrate, RuBP, inhibits this activation process because RuBP strongly binds to the active site of uncarbamylated rubisco. To affect “the activation of the activation,” rubisco activase [60] causes the release of RuBP from uncarbamylated rubisco so that the carbamylation of the lysine by ^ACO₂ can occur. Once activated in this way, RuBP replaces water in the coordination sphere of Mg²⁺ and the Mg²⁺-coordinated RuBP undergoes keto-enol tautomerization, transfers the proton from C(2)–OH the amino group of K175, and replaces this proton by shuttling the proton from C(3)–OH via the carbamate-oxygen of K201 (Scheme 17.2). The resulting metal-coordinated enolate adds the substrate CO₂ (^CCO₂) by nucleophilic addition to form the C(2)–CO₂ bond.

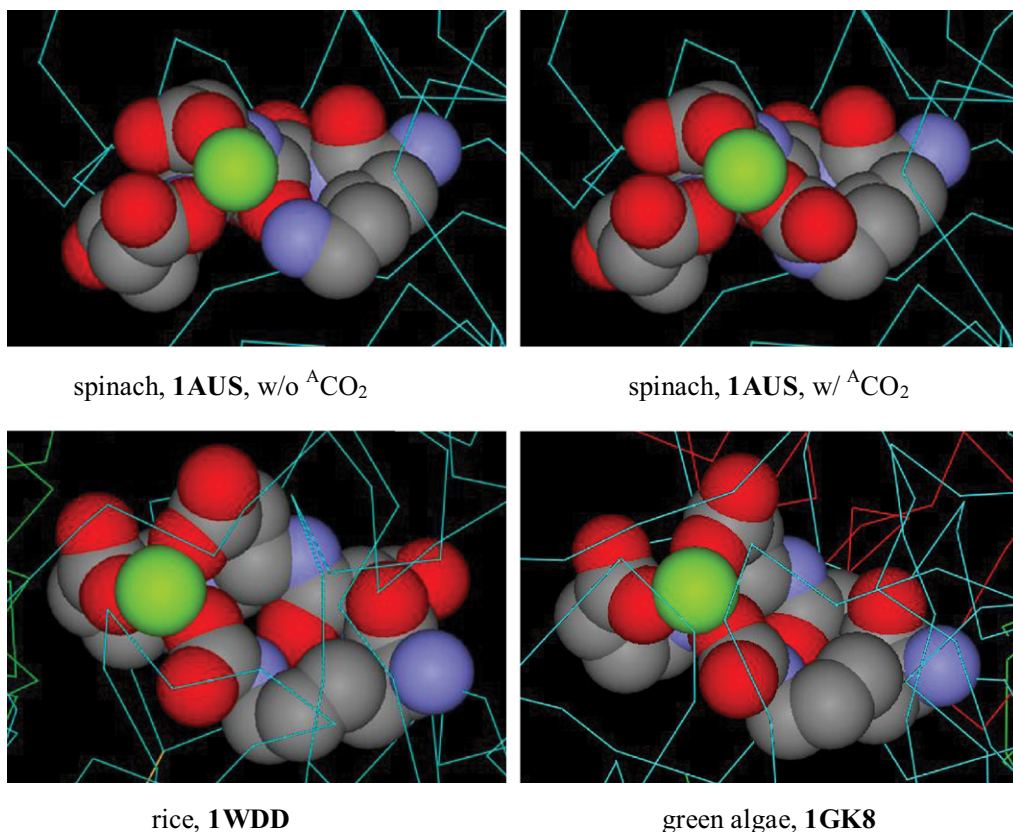


FIGURE 17.1 The crystal structures are shown of activated rubisco in *Spinacia oleracea* [52] without (top, left) and with the display (top, right) of ^ACO₂. Magnesium complexation by the conserved four residue sequence consisting of carbamylated Lys201 (KCX201), Asp202, Asp 203, and Glu204 in the rubisco enzymes of spinach [52], rice [55], and green algae [56].

In their review of the discovery of Rubisco activase [60a] Portis and Salvucci characterized rubisco as “somewhat schizophrenic” because (a) it is bifunctional with its oxygenase activity undoing a considerable amount of carboxylation, (b) one substrate, CO₂, is also an essential activator, and (c) the other substrate, RuBP, also is an inhibitor of the very same activation process. Gutteridge and Pierce [62a] stated “that sometimes perfection may not be immediately obvious” and commented that only the detailed analysis by Tcherkez et al. [62b] reveals “signs of perfection in the slow, nonspecific and discordant activities of Rubisco.”

17.2.2 Rubisco-Based Biomimetic Systems for Reversible CO₂ Capture

One can envision several ways for the construction of rubisco-based biomimetic CO₂ capture systems. One could aim for CO₂ capture and storage and construct biomimetic CCS systems which imitate rubisco’s mechanism of catalysis to capture CO₂ and facilitate the

addition of CO₂ to a RuBP-surrogate. It might be possible to identify a widely available and cheap RuBP-surrogate which does not inhibit rubisco activation and shows a strong bias for carboxylation. Clearly, however, it would be extremely hard to develop such a system given the complexities of rubisco! The availability of sufficient RuBP-surrogate would also always limit the usefulness of this or any other biomimetic CCS system.

We are interested in the development of rubisco-based biomimetic CO₂ capture and release systems (CCR). In CCS systems the captured CO₂ is bound to some substrate and stored as the product of the reaction between CO₂ and that substrate. In CCR systems, on the other hand, CO₂ capture will occur in the open system while CO₂ release will be affected subsequently in a closed system; it is the essential purpose of a CCR system to capture and concentrate CO₂. One can then stockpile captured CO₂ in liquid or solid phase until safe and affordable technologies become available for permanent storage and/or recycling. Captured CO₂ could serve as the basis for a methanol economy [63] and solar-powered CO₂ splitting techniques hold especially great promise [64,65] for sustainable carbon cycling.

One can envision the fabrication of a laminar or porous collection material with large air-accessible functional surfaces to ensure good contact between the air and the chemical CO₂ capture system on the material's large surface. The collection material would capture CO₂ from the air in the open and, when fully loaded with CO₂, the collection material could be retracted into a closed system where CO₂ release would be affected by application of a perturbation (i.e., a temperature increase). Large-scale CO₂ scrubbing would require the deployment of banks of solar-power driven, cycling CCR devices and infrastructure for the periodic collection of captured CO₂ and its storage (*vide supra*). There are many practical and economic issues to address, but it is certainly reasonable to assume that the technical aspects of device design and process control could be solved and that the economic viability of the process largely is a function of thermochemistry of the chemical CO₂ capture system.

It is our goal to develop rubisco-based biomimetic CCR systems for reversible CO₂ capture from air. Our designs of the chemical CO₂ capture and release systems are informed by the understanding of the binding of the activator CO₂, ^ACO₂, in rubisco. The CO₂ capture in a chemical CCR system would occur in the absence of RuBP (or any other related inhibitor) and inhibition of the activation by carbamoylation will not be an issue. Here we discuss the construction of several models, describe the equations for their thermochemical assessment with density functional theory, and we present the results of computational studies of small molecule model systems {CO₂, RNH₂, (A/K), MgL₂} to explore the carbamoylation reaction of the rubisco active site: methylamine (CH₃NH₂) imitates the active site lysine, a simple carbonyl compound (aldehyde or ketone) supplies the hydrogen-bond acceptor function of the amide group of the active site aspartic acid (or asparagine), and magnesium formate MgL₂ serves as a simple model of the Mg²⁺ receptor site. The analysis informs about the thermochemistry of the CO₂ capture reaction and leads to the formulation of general criteria for reversible CO₂ capture systems.

17.3 COMPUTATIONAL METHODS

Potential energy surface (PES) analyses [66] were performed with density functional theory [67]. The hybrid density functional method B3LYP [68] was employed in conjunction with the 6-31G* basis set [69]. All relevant stationary structures were fully optimized and

vibrational frequencies were computed analytically to confirm that the structures are indeed stationary, to determine the character of each stationary structure via its number of imaginary modes, and to determine the thermochemical parameters for this stationary structure.

The potential energy surface, or hypersurface, describes the energy of a molecular assembly and its value depends on the coordinates of all the atoms in the molecular system. It is one of the goals of potential surface analysis to locate so-called stationary structures, that is, structures where the gradients are zero along all of the internal coordinates. A stationary structure is a minimum if a small structural deformation along any one of its internal coordinates increases the energy of the system (positive gradient) and, hence, all of the vibrational frequencies of such a minimum will be positive. A stationary structure will be a saddle point if a small structural deformation along at least one of the internal coordinates decreases the energy of the system (negative gradient) and, hence, a saddle point features at least one imaginary vibrational mode, i.e., a vibrational mode with a negative frequency. A transition state structure corresponds to a first-order saddle point on the potential energy surface and it is characterized by one imaginary vibrational mode (one negative frequency). The process of finding the stationary structures is referred to as structure optimization. Starting with a chemically reasonable initial guess structure, the structure optimization is performed with highly sophisticated algorithms that simultaneously optimize all internal coordinates. For the computational chemist, the art of potential energy surface analysis consists in the formulation of the structural problem and the competent interpretation of the results of the potential energy surface analysis.

The performance of a computational study of a potential energy surface requires the selection of a theoretical level. The theoretical level specifies the specific electronic structure method and the basis set employed in the solution of the Schrödinger equation. The difficult part of any quantum-mechanical electronic structure method concerns the treatment of electron correlation. Sophisticated quantum-mechanical methods for the treatment of electron correlation exist and all of these correlation methods express the correlated wave function as an optimized (most stable) expansion of the ground and excited states of the molecular system. The sophistication of these methods depends on the number of electrons in the active space (and hence the number of excited states considered), on the types of excitations considered (singles, doubles, etc.), on the construction of the expansion (using perturbation theory or variational approaches), and all of these methods are rather computer-time demanding even for small systems. Density functional theory provides for an entirely different approach in that the correlation energy of a given electronic state is thought to depend on the electron density distribution described by the wave function of that one electronic state. The advantage is immediately obvious in that an n -electron correlation problem is replaced by a correlation problem that depends on the electron density distribution and its three Cartesian coordinates. The art of density functional theory consists of the selection of functionals which relate the correlation energy to the electron density distributions. The hybrid density functional method B3LYP has been employed with remarkable success and B3LYP has effectively become the standard DFT method.

The 6-31G* basis set is a so-called polarized, split-valence basis set and this basis set has been widely used with excellent success. A split-valence basis set describes each core orbital by one basis function and each valence orbital by two basis functions. Each basis function of a core orbital consists of a fixed contraction (i.e., a sum) of six Gaussian functions. The inner

basis functions of the valence orbitals are described by fixed contractions of three Gaussian functions and the outer basis function of each valence orbital is a single flat Gaussian function. The 6-31G basis set refers to the ensemble of the exponents of the Gaussian functions of each element and all of the contraction coefficients which have been selected based on analyses of extended sets of molecules. The star in the 6-31G* basis set indicates that the 6-31G basis set has been augmented by sets of d-type functions on all non-hydrogen atoms. It is the purpose of the d-type basis functions to allow for deformations of the p-type orbitals, and it is for this reason that the d-type basis functions are called polarization functions. The use of such a polarized, split-valence basis set is required to adequately describe polar bonds (C=O, C–N, C–O) and dative bonding (Mg²⁺ complexation). All of the models studied here are overall neutral systems. In particular, all formate ions always appear as neutral ion pairs with the magnesium counterion. While the description of anions would require additional augmentation of the basis set with so-called diffuse functions (spatially extended s- and p-type basis functions), an adequate description of overall neutral ion pairs is possible with the standard 6-31G* basis set.

Molecular models of the optimized structures are shown in the figures, selected structural parameters are provided in the figure legends and discussed in the text, and Cartesian coordinates of all optimized structures are provided as Supporting Information. Total energies (E_{tot}), vibrational zero point energies (VZPE), thermal energies (TE), molecular entropies (S), the numbers of imaginary frequencies (NI), and the lowest vibrational frequencies ν_1 and the dipole moments μ are given in Table 17.1. Pertinent relative and reaction

TABLE 17.1 Total Energy and Thermochemical Data (a)

Molecule	E_{tot}	VZPE	TE	S	ν_1	μ
<i>Small systems</i>						
O=C=O	–188.580940	6.36	8.23	39.63	640	0.000
H ₂ O	–76.408953	13.28	15.06	45.14	1713	2.095
CH ₃ NH ₂ (=MA)	–95.853205	40.43	42.55	57.29	332	1.472
Mg(O ₂ CH) ₂ (=MgL ₂)	–578.568463	30.35	35.04	86.79	65	0.006
H ₂ CO (=FA)	–114.500473	16.83	18.63	52.24	1190	2.187
(CH ₃) ₂ CO (=Ac)	–193.155695	52.76	56.16	73.64	37	2.815
CH ₃ NH ₂ ·OCH ₂	–210.361237	58.74	63.37	84.04	46	0.942
CH ₃ NH ₂ ·OC(CH ₃) ₂	–289.017622	94.41	100.85	103.44	17	1.969
CH ₃ NH ₂ ·CO ₂	–284.440170	48.40	53.07	87.87	22	2.130
H ₂ O·CO ₂	–264.995337	21.50	25.59	80.40	30	2.246
L ₂ Mg·CO ₂	–767.159793	38.23	45.46	110.95	31	2.388
L ₂ Mg·OH ₂	–655.014059	45.67	52.35	102.57	41	4.541
CH ₃ NH ₂ ·OH ₂	–172.276175	56.13	60.11	75.88	99	3.414
FA·OH ₂	–190.920279	32.59	36.16	71.56	155	2.347
Ac·OH	–269.578515	68.34	73.64	89.17	34	3.765

(Continued)

TABLE 17.1 (Continued)

Molecule	E_{tot}	VZPE	TE	S	ν_1	μ
<i>NMCA</i>						
trans-trans, C_{1v} 1	-284.440091	50.25	53.83	75.08	90	2.539
trans-cis, C_{sv} 2	-284.442125	50.11	53.77	76.42	47	2.341
cis-trans, C_{1v} 3	-284.427557	49.87	53.50	75.18	91	5.348
cis-cis, C_{sv} 4a	-284.427958	49.26	52.79	75.42	-298	5.256
cis-cis, C_{1v} 4b	-284.429028	49.86	53.50	75.19	85	4.852
<i>NMCA-O=CH₂</i>						
trans-trans, C_{sv} 5	-398.954858	68.63	74.72	98.92	30	0.171
trans-cis, C_{sv} 6	-398.953433	68.35	74.62	101.26	35	3.468
cis-trans, C_{sv} 7	-398.943402	68.24	74.37	98.52	39	3.071
cis-cis, C_{sv} 8a	-398.943844	67.76	73.82	100.58	-142	8.002
cis-cis, C_{1v} 8b	-398.944304	68.04	74.47	104.50	21	7.818
<i>NMCA-O=C(CH₃)₂</i>						
trans-trans, C_{sv} 9a	-477.611017	104.02	111.48	111.79	-25	2.148
trans-trans, C_{1v} 9b	-477.611038	104.12	112.10	117.54	21	2.119
trans-cis, C_{sv} 10a	-477.610108	103.88	111.44	113.22	-21	5.191
trans-cis, C_{1v} 10b	-477.610102	103.88	112.03	121.57	11	5.184
cis-trans, C_{sv} 11a	-477.599661	103.60	111.12	112.35	-28	4.020
cis-trans, C_{1v} 11b	-477.599692	103.72	111.74	117.19	22	3.993
cis-cis, C_{sv} 12a	-477.604295	103.63	110.75	111.39	-31	8.514
cis-cis, C_{1v} 12b	-477.604905	104.04	112.03	117.43	21	7.703
<i>NMCA-MgL₂</i>						
tr.-tr., OHO, 13a	-863.062346	81.86	90.83	123.02	34	6.285
tr.-tr., NHO, 13b	-863.057174	81.90	90.97	124.29	29	6.107
tr.-cis, OHO, 14a	-863.063258	81.88	90.84	122.92	34	6.021
trans-cis, 14b	-863.050893	81.71	90.93	125.98	21	6.409
cis-trans, 15a	-863.035216	81.09	90.52	128.64	20	10.166
cis-tr., NHO, 15b	-863.045882	81.61	90.67	123.11	29	8.383
cis-cis, 16a	-863.035548	81.02	90.50	129.15	23	9.634
cis-cis, 16b	-863.037748	81.31	90.65	126.66	16	8.792

(Continued)

TABLE 17.1 (Continued)

Molecule	E_{tot}	VZPE	TE	S	ν_1	μ
<i>NMCA·MgL₂·FA</i>						
trans-trans, 17a	-977.579366	100.24	111.77	145.31	24	3.982
trans-trans, 17b	-977.580010	100.46	111.88	143.91	24	3.512
trans-trans, 17c	-977.572878	100.29	111.78	145.40	23	4.666
trans-trans, 17d	-977.581032	100.34	111.63	140.22	28	5.989
trans-trans, 17e	-977.568154	100.13	111.82	146.80	23	4.700
trans-trans, 17f	-977.575560	100.42	111.77	140.33	28	6.238
trans-cis, 18a	-977.576781	100.03	111.68	147.93	19	6.571
trans-cis, 18b	-977.574027	100.12	111.72	146.20	17	4.174
<i>NMCA·MgL₂·Ac</i>						
trans-trans, 21a	-1056.236362	135.91	149.17	159.68	19	4.543
trans-trans, 21b	-1056.225166	135.46	149.08	164.99	15	4.922

(a) Total energies E_{tot} in atomic units (1 a.u. = 627.51 kcal/mol), vibrational zero-point energies VZPE (in kcal/mol), thermal energies TE (in kcal/mol), and molecular entropies S (in cal K⁻¹ mol⁻¹). The lowest vibrational frequency ν_1 is provided as a wave number (in cm⁻¹) and the molecular dipole moment is given in Debye.

energies (in kcal/mol) are listed in Table 17.2 and four thermodynamic values are provided for each parameter, and these are ΔE , $\Delta H_0 = \Delta E + \Delta \text{VZPE}$, $\Delta H_{298} = \Delta E + \Delta \text{TE} + \Delta(pV)$, and $\Delta G_{298} = \Delta H_{298} + 298.15 \cdot \Delta S$.

All of the computed thermodynamic parameters describe gas phase chemistry, that is, the computed data describe the stabilities of free molecules and their aggregation and/or complexation in vacuum. Yet, we are interested in condensed phase chemistry and to attach

TABLE 17.2 Relative and reaction energies (a)

	Relation/Reaction	ΔE	ΔH_0	ΔH_{298}	ΔG_{298}
<i>Aggregates w/o NMCA</i>					
R3a	CH ₃ NH ₂ + FA → CH ₃ NH ₂ ·FA	-4.74	-3.27	-2.56	5.04
R3b	CH ₃ NH ₂ + Ac → CH ₃ NH ₂ ·Ac	-5.47	-4.25	-3.34	4.86
R3c	CH ₃ NH ₂ + CO ₂ → CH ₃ NH ₂ ·CO ₂	-3.78	-2.17	-1.49	1.20
R7	L ₂ Mg + CO ₂ → L ₂ Mg·CO ₂	-6.52	-5.01	-4.33	0.28
H1	CH ₃ NH ₂ + H ₂ O → CH ₃ NH ₂ ·HOH	-8.80	-6.38	-6.29	1.62
H2	FA + H ₂ O → FA·HOH	-6.81	-4.34	-4.34	3.35
H3	Ac + H ₂ O → Ac·HOH	-8.70	-6.40	-6.28	2.55
H4	CO ₂ + H ₂ O → H ₂ O·CO ₂	-3.42	-1.55	-1.12	0.18
R9	L ₂ Mg + OH ₂ → L ₂ Mg·OH ₂	-22.99	-20.96	-20.74	-11.99
R10	L ₂ Mg·OH ₂ + CO ₂ → L ₂ Mg·CO ₂ + OH ₂	16.47	15.95	16.42	12.28

(Continued)

TABLE 17.2 (Continued)

	Relation/Reaction	ΔE	ΔH_0	ΔH_{298}	ΔG_{298}
<i>NMCA isomers</i>					
	1 vs. 2	1.28	1.42	1.34	1.74
	3 vs. 2	9.14	8.90	8.87	9.24
	4 vs. 2	8.22	7.97	7.95	8.32
R1	$\text{CH}_3\text{NH}_2 + \text{CO}_2 \rightarrow \mathbf{2}$	-5.01	-1.69	-2.02	4.09
R3c	$\text{CH}_3\text{NH}_2 + \text{CO}_2 \rightarrow \text{CH}_3\text{NH}_2 \cdot \text{CO}_2$	-3.78	-2.17	-1.49	1.20
R1'	$\text{CH}_3\text{NH}_2 \cdot \text{CO}_2 \rightarrow \mathbf{2}$	-1.23	0.49	-0.53	2.89
<i>E_{rel}, NMCA·(A/K) isomers</i>					
	FA, 6 vs. 5	0.89	0.62	0.79	0.09
	FA, 7 vs. 5	7.19	6.80	6.84	6.96
	FA, 8b vs. 5	6.62	6.04	6.37	4.71
	Ac, 10b vs. 9b	0.59	0.35	0.51	-0.69
	Ac, 11b vs. 9b	7.12	6.71	6.76	6.86
	Ac, 12b vs. 9b	3.85	3.77	3.77	3.80
<i>E_{br}, NMCA·Fc isomers</i>					
	trans-trans, 1 + FA → 5	-8.97	-7.42	-6.71	1.76
	trans-cis, 2 + FA → 6	-6.80	-5.39	-4.58	3.59
	cis-trans, 3 + FA → 7	-9.65	-8.11	-7.40	1.22
	cis-cis, 4b + FA → 8b	-9.29	-7.94	-6.95	-0.11
R2a	2 + FA → 5	-7.69	-6.01	-5.37	3.50
R3a	$\text{CH}_3\text{NH}_2 + \text{FA} \rightarrow \text{CH}_3\text{NH}_2 \cdot \text{FA}$	-4.74	-3.27	-2.56	5.04
R4a	$\text{CH}_3\text{NH}_2 \cdot \text{FA} + \text{CO}_2 \rightarrow \mathbf{5}$	-7.96	-4.43	-4.83	2.54
<i>E_{br}, NMCA·Ac isomers</i>					
	trans-trans, 1 + Ac → 9b	-9.57	-8.46	-7.46	1.83
	trans-cis, 2 + Ac → 10b	-7.71	-6.70	-5.61	2.89
	cis-trans, 3 + Ac → 11b	-10.32	-9.23	-8.23	1.20
	cis-cis, 4b + Ac → 12b	-12.66	-11.24	-10.30	-0.94
R2b	2 + Ac → 9b	-8.29	-7.04	-6.12	3.58
R3b	$\text{CH}_3\text{NH}_2 + \text{Ac} \rightarrow \text{CH}_3\text{NH}_2 \cdot \text{Ac}$	-5.47	-4.25	-3.34	4.86
R4b	$\text{CH}_3\text{NH}_2 \cdot \text{Ac} + \text{CO}_2 \rightarrow \mathbf{9b}$	-7.83	-4.47	-4.81	2.81
<i>E_{rel}, NMCA·MgL₂ isomers</i>					
	trans-trans, 13a vs. 14a	0.57	0.55	0.56	0.53
	trans-trans, 13b vs. 14a	3.82	3.84	3.94	3.54

(Continued)

TABLE 17.2 (Continued)

	Relation/Reaction	ΔE	ΔH_0	ΔH_{298}	ΔG_{298}
	trans-cis, 14b vs. 14a	7.76	7.59	7.85	6.93
	cis-trans, 15a vs. 14a	17.60	16.81	17.27	15.56
	cis-trans, 15b vs. 14a	10.90	10.63	10.73	10.67
	cis-cis, 16a vs. 14a	17.39	16.53	17.04	15.19
	cis-cis, 16b vs. 14a	16.01	15.44	15.81	14.70
<i>E_b, NMCA·MgL₂ isomers</i>					
	1 + MgL ₂ → 13a	-33.76	-32.51	-31.80	-20.22
	1 + MgL ₂ → 13b	-30.51	-29.21	-28.41	-17.21
R5	2 + MgL ₂ → 14a	-33.05	-31.64	-31.02	-19.00
	2 + MgL ₂ → 14b	-25.29	-24.05	-23.17	-12.07
	3 + MgL ₂ → 15a	-24.60	-23.72	-22.62	-12.68
	3 + MgL ₂ → 15b	-31.29	-29.90	-29.16	-17.57
	4b + MgL ₂ → 16a	-23.88	-23.08	-21.92	-12.13
	4b + MgL ₂ → 16b	-15.26	-24.16	-23.15	-12.63
R6	CO ₂ + CH ₃ NH ₂ + MgL ₂ → 14a	-38.06	-33.32	-33.04	-14.92
R7	L ₂ Mg + CO ₂ → L ₂ Mg·CO ₂	-6.52	-5.01	-4.33	0.28
R8	CO ₂ ·MgL ₂ + CH ₃ NH ₂ → 14a	-31.54	-28.32	-28.71	-15.20
R9	L ₂ Mg + OH ₂ → L ₂ Mg·OH ₂	-22.99	-20.96	-20.74	-11.99
R10	L ₂ Mg·OH ₂ + CO ₂ → L ₂ Mg·CO ₂ + OH ₂	16.47	15.95	16.42	12.28
R11	H ₂ O·MgL ₂ + CO ₂ + CH ₃ NH ₂ → 14a	-15.06	-12.36	-12.29	-2.92
<i>NMCA·MgL₂·FA isomers</i>					
	17b vs. 17a	-0.40	-0.19	-0.29	0.13
	17c vs. 17a	4.07	4.11	4.09	4.06
	17d vs. 17a	-1.05	-0.95	-1.18	0.33
	17e vs. 17b	7.44	7.11	7.38	6.52
	17f vs. 17b	2.79	2.75	2.69	3.76
	18b vs. 18a	1.73	1.81	1.77	2.29
	18a vs. 17a	1.62	1.41	1.54	0.76
R12a	14a + FA → 17a	-9.81	-8.28	-7.52	1.38
R14a	H ₂ O·MgL ₂ + CO ₂ + MA·FA → 17a + H ₂ O	-20.13	-17.38	-17.26	-6.59
<i>NMCA·MgL₂·Ac isomers</i>					
	21b vs. 21a	7.03	6.58	6.94	5.36
R12b	14a + Ac → 21a	-10.93	-9.66	-8.76	2.24
R14b	H ₂ O·MgL ₂ + CO ₂ + MA·Ac → 21a + H ₂ O	-20.52	-17.76	-17.72	-5.54

(a) All energies are given in kcal/mol. Numbers are provided to two digits for numerical accuracy at the selected theoretical level.

meaning to the computed data requires some thought. To begin with, we point out that we computed the ΔH_{298} values assuming that the term $\Delta(pV)$ is negligible. If one is interested in volume effects of reactions that convert n molecule to m molecules, one can easily compute the respective enthalpy of the gas-phase reaction by addition of $(m-n)\cdot RT$ to ΔH_{298} (where $RT=0.595$ kcal/mol). A more important issue concerns the molecular entropies. The computed molecular entropies are sums of the entropies due to translational, rotational, and vibrational motions. The translational and rotational entropies are large; their sum exceeds the vibrational entropies for small molecules (i.e., NMCA) and their sum still matches the vibrational entropy of our largest systems (i.e., **21**). The point here is that the translational and rotational freedoms of molecules in condensed phase are quite obviously reduced as compared to the gas phase. If all of the computed molecular entropies S are overestimated, then one must wonder about the consequence for ΔS of an association reaction. The translational and rotational entropies in condensed phase decrease with molecular size and, hence, the overestimation of the computed molecular entropy is larger for an aggregate than for its constituents and the computed ΔS value for an aggregate formation reaction is systematically overestimated. The ΔS value for an aggregation usually is negative and the $-T\cdot\Delta S$ term increases ΔG relative to the ΔH term. If the molecular entropy of the aggregate is overestimated the most, then the computed ΔS value for an aggregate formation reaction will not be negative enough and, in turn, the ΔG value for this aggregation will not be raised enough relative to the ΔH term. Hence, the computed ΔG values of aggregation reactions are lower limits.

Computations were performed with *Gaussian09* [70] in conjunction with *Gaussview 5* [71], on an SGI Altix BX2 SMP system with 64 Itanium2 processors and a Dell EM64T cluster system with 512 processors.

17.4 RESULTS AND DISCUSSION

17.4.1 Small Molecule Models: Model Construction and Thermochemistry

17.4.1.1 Overview and Conception of the Approach

We want to evaluate the environmental effects on the thermochemistry of the addition of methylamine to carbon dioxide to form *N*-methylcarbaminic acid (NMCA) in the gas phase (*g*), reaction **R1**. Two effects of the environment will be considered and these are the stabilization of the product by hydrogen-bonding between NMCA and a model carbonyl compound and the complexation of the NMCA molecule by a model magnesium complex. We will first model each one of these two effects separately and subsequently we will also examine the consequences of the combination of both effects together. The thermochemistry of the model systems will be described by a system of 14 reactions which are introduced here.



The evaluation of the equations requires the determination of the structures and the energies of NMCA, of its aggregates NMCA·(A/K) and complexes NMCA·MgL₂, and of the complexes NMCA·MgL₂·(A/K). Therefore, in the following sections of this chapter we will report on the isomers **1–4** of NMCA, the isomers **5–8** of the formaldehyde aggregates NMCA·FA, the isomers **9–12** of the acetone aggregates NMCA·Ac, the isomers **13–16** of the complexes NMCA·MgL₂, and the isomers **17** and **18** of the complex NMCA·MgL₂·FA and structures **21** of the complex

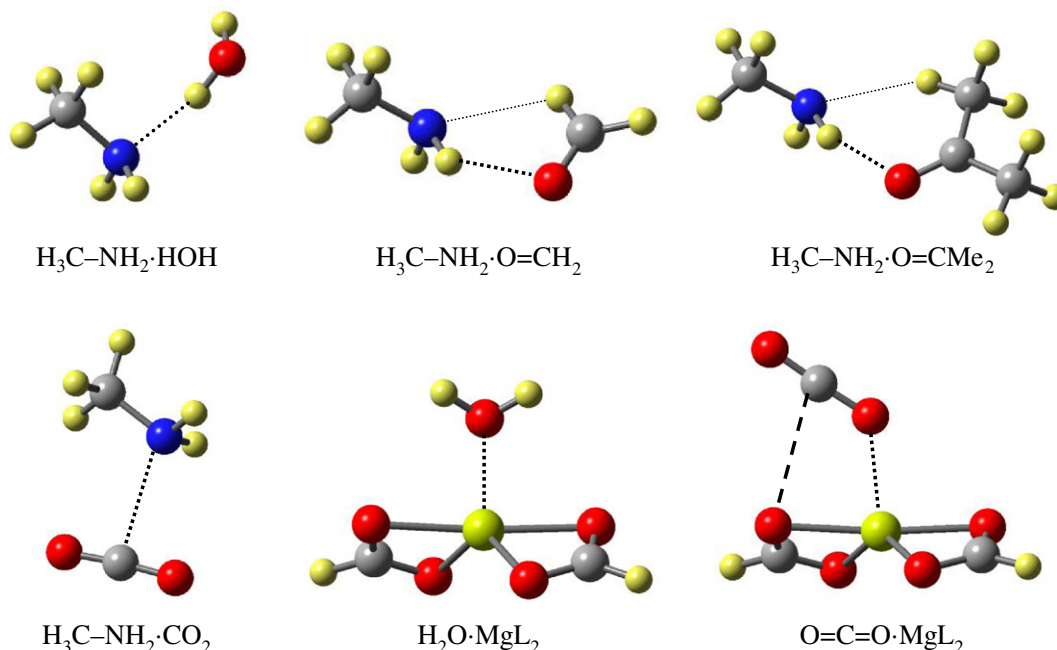


FIGURE 17.2 Structures of aggregates formed by methylamine CH_3NH_2 with formaldehyde, acetone, CO_2 , and water, and of complexes formed between magnesium formate MgL_2 and water and CO_2 . Major structural parameter (in Å and degrees) describing the intermolecular bonding situation: $\text{H}_3\text{C-NH}_2 \cdot \text{HOH}$: $d(\text{N} \cdots \text{HO}) = 1.920$; $\text{H}_3\text{C-NH}_2 \cdot \text{O=CH}_2$: $d(\text{NH} \cdots \text{O}) = 2.260$, $d(\text{N} \cdots \text{H-CHO}) = 2.561$; $\text{H}_3\text{C-NH}_2 \cdot \text{O=CMe}_2$: $d(\text{NH} \cdots \text{O}) = 2.180$, $d(\text{N} \cdots \text{H-CH}_2) = 2.524$; $\text{H}_3\text{C-NH}_2 \cdot \text{O=C=O}$: $d(\text{N} \cdots \text{CO}_2) = 2.802$; $\text{H}_2\text{O} \cdot \text{MgL}_2$: $d(\text{Mg} \cdots \text{O}) = 2.070$; $\text{O=C=O} \cdot \text{MgL}_2$: $d(\text{Mg} \cdots \text{O}) = 2.239$, $\angle(\text{Mg-O-C}) = 127.7$, INA distance $d(\text{O}_2\text{C} \cdots \text{O}_{\text{formate}}) = 2.903$.

$\text{NMCA} \cdot \text{MgL}_2 \cdot \text{Ac}$. The discussion and the evaluation of these equations also require the determination of several smaller systems, and the structures and energies were determined of the substrates methylamine CH_3NH_2 and CO_2 , of the aggregates of methylamine with formaldehyde, acetone, and CO_2 , and of magnesium formate MgL_2 and its complexes $\text{CO}_2 \cdot \text{MgL}_2$ and $\text{H}_2\text{O} \cdot \text{MgL}_2$. The energies of the small systems are listed on top of Table 17.1, the structures of some of the small systems are shown in Figure 17.2, and the aggregation energies of these systems (reactions R3, R7, and R9) will be discussed below in the appropriate context.

17.4.1.2 Modeling the Hydrogen-Bond Acceptor Carbonyl Site

The model carbonyl compound will be an aldehyde (A) or a ketone (K) and we consider one example of each. In reactions (R2)–(R4) we write (A/K) for the model carbonyl compound, and (R2)–(R4) will be evaluated for formaldehyde (R2a–R4a) and for acetone (R2b–R4b).



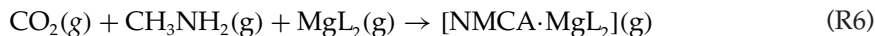
Reaction R2 describes the association of NMCA with the model carbonyl compound (A/K) and we refer to the aggregate as NMCA·(A/K). The presence of the carbonyl compound will not only stabilize the addition product NMCA but the carbonyl also has the potential to stabilize the amine substrate before the addition reaction. Reaction R3 describes the association of the substrate methylamine with the model carbonyl compound (A/K) and we refer to this pre-reaction substrate aggregate as CH₃NH₂·(A/K). The combined effects of substrate and product stabilization by the carbonyl compound are reflected in reaction R4, the addition of CO₂ to a carbonyl-aggregated methylamine to form the carbonyl-aggregated *N*-methylcarbaminic acid. The thermochemistry of reaction R4 is a function of reactions (R1)–(R3): R4 = R1 + R2 – R3.



We evaluated reaction R3 for formaldehyde (R3a) and acetone (R3b). The major intermolecular contact in the aggregates CH₃NH₂·O=CH₂ and CH₃NH₂·O=CMe₂ (Figure 17.2) is the hydrogen-bonding interaction between one amino-H and the carbonyl-O. In addition, there are secondary, weaker contacts between the amino-N and an H-atom of the carbonyl compound with similar contact distances in the formaldehyde system ($d(\text{N} \cdots \text{H}-\text{CHO}) = 2.561 \text{ \AA}$) and in the acetone system ($d(\text{N} \cdots \text{H}-\text{CH}_2\text{COMe}) = 2.524 \text{ \AA}$). Overall, these CH contacts are relatively weak ($\Delta H_{298}(\text{R3a}) = -2.6 \text{ kcal/mol}$, $\Delta H_{298}(\text{R3b}) = -3.3 \text{ kcal/mol}$) and both associations are heavily disfavored by the association entropy ($\Delta G_{298}(\text{R3a}) \approx \Delta G_{298}(\text{R3b}) \approx +5.0 \text{ kcal/mol}$).

17.4.1.3 Modeling the Magnesium Complex Site

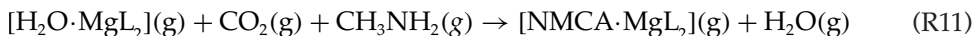
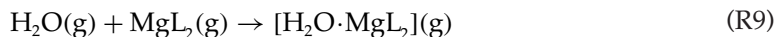
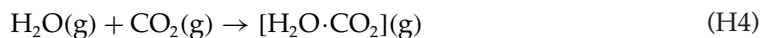
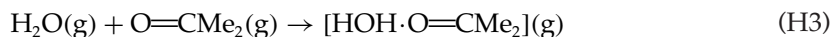
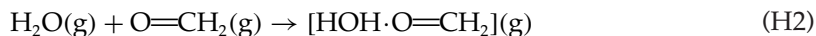
The model magnesium complex will be a neutral complex MgL₂ where L is a singly charged anion, and we model MgL₂ with magnesium formate (L = HCO₂⁻). Reaction R5 describes the association of NMCA with the model magnesium complex MgL₂ to form the complex NMCA·MgL₂. The presence of the magnesium formate will not only stabilize the addition product NMCA but the magnesium formate also has the potential to stabilize the CO₂ substrate before the addition reaction. Reaction R7 describes the association of the substrate CO₂ with the model magnesium complex MgL₂ to form the pre-reaction substrate aggregate CO₂·MgL₂. The combined effects of CO₂ substrate and NMCA product stabilization by the model magnesium complex are reflected in reaction R8, the addition of methylamine to a Mg²⁺-complexed CO₂ molecule to form the Mg²⁺-complexed *N*-methylcarbaminic acid. The thermochemistry of reaction R8 is a function of reactions R1, R5, and R7: R8 = R1 + R5 – R7 and with R6 = R1 + R5 one obtains R8 = R6 – R7.



The structure of the product $\text{CO}_2 \cdot \text{MgL}_2$ of the association reaction R7 is shown in Figure 17.2. The CO_2 molecule coordinates to the Mg^{2+} cation with a ligand distance $d(\text{Mg} \cdots \text{O}) = 2.239 \text{ \AA}$ and at an angle $\angle(\text{Mg}-\text{O}-\text{C}) = 127.7^\circ$. The geometry of the complex also suggests an attractive interaction between the electrophilic center of the CO_2 ligand and the proximate formate O-atom. This interaction is indicated in Figure 17.2 by the long-dash line and the incipient nucleophilic attack (INA, [72]) distance between the nucleophilic and electrophilic centers is about 2.09 \AA . Carbon dioxide is a highly quadrupolar molecule [42] and one might expect its interaction with a Mg^{2+} cation to be strong. Yet, the computations suggest that the complexation of CO_2 by magnesium formate is exothermic by only $\Delta H_{298}(\text{R7}) = -4.3 \text{ kcal/mol}$ and that the association is essentially thermoneutral on the free enthalpy surface with $\Delta G_{298}(\text{R7}) = +0.3 \text{ kcal/mol}$.

17.4.1.4 Modeling Water/ CO_2 Exchange at the Magnesium Complex Site

Prior to the addition reaction, the substrates methylamine and CO_2 and their future binding sites, the model carbonyl compound, and the model magnesium complex, all will be interacting with their respective environments as best as possible. These interactions might involve some specific interactions (i.e., the carbonyl group in rubisco could engage in hydrogen-bonding with HB-donors in the peptide chain) but hydrogen-bonding with water molecules is most likely. The interactions of one water molecule with CH_3NH_2 , formaldehyde, acetone, or CO_2 (reactions H1–H4) all are relatively weak whereas the complexation of MgL_2 by water (reaction R9) stands out dramatically.

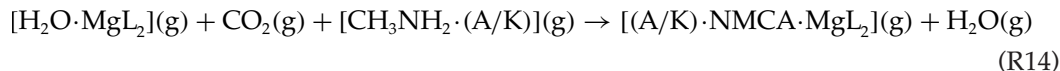
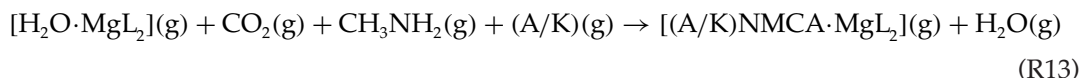
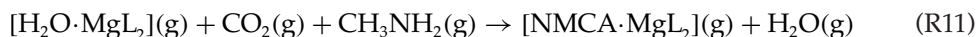


As expected, the formations of the hydrates $\text{CH}_3\text{NH}_2 \cdot \text{HOH}$ ($\Delta H_{298}(\text{H1}) = -6.3 \text{ kcal/mol}$), $\text{H}_2\text{C}=\text{O} \cdot \text{HOH}$ ($\Delta H_{298}(\text{H2}) = -4.3 \text{ kcal/mol}$), $\text{Me}_2\text{C}=\text{O} \cdot \text{HOH}$ ($\Delta H_{298}(\text{H3}) = -6.3 \text{ kcal/mol}$), and $\text{H}_2\text{O} \cdot \text{CO}_2$ ($\Delta H_{298}(\text{H4}) = -1.2 \text{ kcal/mol}$) are slightly exothermic, but the data in Table 17.2 also show that all of these aggregations are slightly endergonic, $\Delta G_{298}(\text{H}\%) > 0$. On the other hand, the complex formed by association of one water molecule with magnesium formate is stable enough to have some lifetime: reaction R9 is highly exothermic ($\Delta H_{298}(\text{R9}) = -20.7 \text{ kcal/mol}$) and the reaction also is significantly exergonic ($\Delta G_{298}(\text{R9}) = -12.0 \text{ kcal/mol}$).

The comparison of reactions **R7** and **R9** shows that the complexations of substrate CO₂ and of water by MgL₂ will be very different and, consequently, the exchange of a ligand water by a CO₂ molecule, reaction **R10** (R10 = R7 – R9) is significantly endothermic ($\Delta H_{298}(\text{R10}) = 16.4 \text{ kcal/mol}$) and endergonic ($\Delta G_{298}(\text{R10}) = 12.3 \text{ kcal/mol}$). Therefore, a reasonable model of the Mg²⁺-catalyzed *N*-methylcarbaminic acid formation must consider the forced replacement of ligand water by CO₂ and, hence, reaction **R10** presents a much more appropriate model than reaction **R8**. Accounting for reaction **R10** converts reaction **R8** to reaction **R11**: R11 = R8 + R10.

17.4.1.5 Modeling the HB-Acceptor Carbonyl and Magnesium Complex Sites

We are now ready to consider the combined effects of product stabilization by hydrogen-bonding between NMCA and a model carbonyl compound and by complexation of NMCA by the model magnesium complex.



We constructed the model systems (A/K)·NMCA·MgL₂ by addition of formaldehyde or acetone to the appropriate magnesium formate complexes NMCA·MgL₂, and reaction **R12** describes these associations for formaldehyde (R12a) and acetone (R12b). Combination of reactions **R11** and **R12** results in reaction **R13** (R13 = R11 + R12), and considering the aggregation between the substrate methylamine and the carbonyl model (reaction **R3**) one obtains reaction **R14**; R14 = R13 – R3 = R11 + R12 – R3. Reaction **R14** models the capture of CO₂ and the addition of the Mg²⁺-complexed CO₂ to a pre-positioned, carbonyl-aggregated methylamine CH₃NH₂·(A/K) to form the Mg²⁺-complexed and carbonyl-aggregated *N*-methylcarbaminic acid (A/K)·NMCA·MgL₂.

17.4.2 Stereochemistry of *N*-Methylcarbaminic Acid

N-Methylcarbaminic acid (NMCA) is able to form isomers about the CN bond due to amide resonance. The labels *trans* and *cis* are used to describe the relation between the *N*-methyl and the carbonyl groups in the CN-isomers. With a view to the potential for metal complexation of both oxygen atoms of NMCA's carboxylic acid group, we studied not only the "normal" carboxylic acid isomers with the H₂NC(O)–OH conformation in which the acid-H is *trans* relative to the amino group but we also considered the uncommon *cis* isomer. The first and second stereochemical labels describe the stereochemistry about the MeNHC(O)–OH and

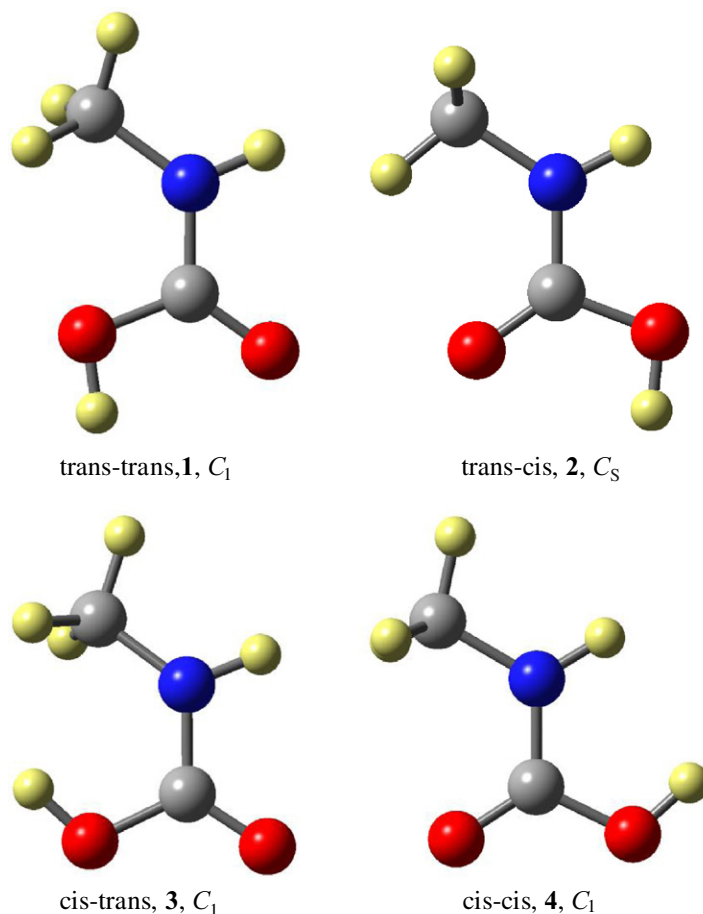


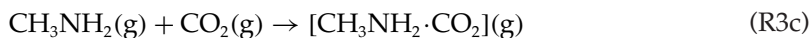
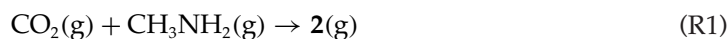
FIGURE 17.3 Molecular models of the optimized structures of the stereoisomers of *N*-methylcarbaminic acid (NMCA). The first and second stereochemical labels describe the stereochemistry about the MeNHC(O)–OH and MeNH–C(O)OH bonds, respectively. Major structural parameter (in Å and degrees): $d(\text{C–N})$: 1.361 (**1**), 1.358 (**2**), 1.380 (**3**), and 1.382 (**4b**); $d(\text{C=O})$: 1.218 (**1**), 1.219 (**2**), 1.210 (**3**), and 1.209 (**4**); $d(\text{C–OH})$: 1.366 (**1**), 1.368 (**2**), 1.364 (**3**), and 1.368 (**4**); $\angle(\text{O=C–OH})$: 123.0 (**1**), 123.1 (**2**), 121.0 (**3**), and 121.0 (**4**); $\angle(\text{O=C–N})$: 125.2 (**1**), 126.6 (**2**), 123.5 (**3**), and 124.7 (**4**); $\angle(\text{C–N–CH}_3)$: 125.7 (**1**), 122.5 (**2**), 125.7 (**3**), and 118.6 (**4**); $\angle(\text{O=C–N–H})$: 7.7 (**1**), 180.0 (**2**), 8.1 (**3**), and -153.4 (**4**); $\angle(\text{O=C–N–CH}_3)$: 171.9 (**1**), 0.0 (**2**), 163.4 (**3**), and -7.5 (**4**).

MeNH–C(O)OH bonds, respectively. The four possible isomers **1–4** of *N*-methylcarbaminic acid were located and molecular models of the optimized structures are shown in [Figure 17.3](#).

Except for the C_s -symmetric structure **2**, the structures of the minima are asymmetric (C_1) because the amide-N is slightly pyramidal in those isomers; the dihedral angles $\angle(\text{O=C–N–H})$ are 7.7° (**1**), 180° (**2**), 8.1° (**3**), and -153.4° (**4**), and the dihedrals $\angle(\text{O=C–N–CH}_3)$ are 171.9° (**1**), 0° (**2**), 163.4° (**3**), and -7.5° (**4**). *N*-Inversion in isomers **1**, **3**, and **4** is extremely easy, and their actual structures are best thought of as fluxional molecules that oscillate between their respective enantiomers. The most stable isomer is the trans-cis structure **2** with a small

preference over the trans-trans isomer **1**. The two “normal” trans-acid isomers **1** and **2** are clearly favored over the cis-acid isomers **3** and **4** by about 8–10 kcal/mol (Table 17.2).

The evaluation of the addition reaction $\text{CH}_3\text{NH}_2 + \text{CO}_2 \rightarrow \text{NMCA}$ (R1) with the data for the most stable isomer **2** of *N*-methylcarbaminic acid shows reaction R1 to be slightly exothermic ($\Delta H_{298}(\text{R1}) = -2.0$ kcal/mol) but also slightly endergonic ($\Delta G_{298}(\text{R1}) = +4.1$ kcal/mol). Hence, the addition of methylamine to carbon dioxide is thermodynamically unfavorable and this result is in agreement with reports of earlier, similar studies [73–76]. We computed the thermodynamic parameters with the approximation $\Delta(pV) \approx 0$ which applies to the condensed phase reaction of methylamine with dissolved CO₂. For the addition of gaseous CO₂ and methylamine, one would have to modify ΔH_{add} and ΔG_{add} by addition of $\Delta(pV) \approx -RT = -0.6$ kcal/mol and the reaction free enthalpy would then become $\Delta G_{\text{add}} = 3.5$ kcal/mol, and it would still be positive.



The optimized structure of the aggregate $\text{CH}_3\text{NH}_2 \cdot \text{CO}_2$ is shown in Figure 17.2. The amine-N approaches the electrophilic center of CO₂ to about 2.8 Å and CO₂ remains almost linear (175.0°). The association reaction R3c is only slightly exothermic ($\Delta H_{298}(\text{R3c}) = -1.5$ kcal/mol) and it is also slightly endergonic ($\Delta G_{298}(\text{R3c}) = +1.2$ kcal/mol). Aggregate $\text{CH}_3\text{NH}_2 \cdot \text{CO}_2$ does not present a stable resting state, but the addition reaction proceeds through structures of this type on the way to the reaction transition state of the addition reaction.

17.4.3 Carbonyl-Aggregates of *N*-Methylcarbaminic Acid

Hydrogen-bonding of the carbamide-H presents one way to stabilize the addition product NMCA. We explored the structures and stabilities of aggregates formed between NMCA and two model carbonyls as hydrogen-bond acceptors. Formaldehyde (FA) contains rather positively charged H-atoms which might engage in additional H-bonding. This potential disadvantage is avoided, or at least significantly reduced, with the use of acetone (Ac) as model carbonyl compound. The H-bonded aggregates **5–8** and **9–12**, formed between isomers **1–4** and FA and Ac, respectively, are shown in Figures 17.4–17.6, respectively.

We have seen that the isomers **1**, **3**, and **4** of *N*-methylcarbaminic acid are asymmetric and that their enantiomerizations are very fast. The results are pretty much the same whether the C_s-symmetric structure **2** is undergoing *N*-inversion vibrations or whether a non-planar structure is oscillating between its enantiomers. Similar issues occur with the carbonyl-aggregates and the potential energy surface characteristics might differ from one case to the next, but the underlying physical reality remains essentially the same. The NMCA·FA adducts **5–7** feature C_s-symmetric minima while adduct **8** is slightly asymmetric. On the other hand, the NMCA·Ac adducts **9–12** all feature asymmetric minima (C₁) and nearly isoenergetic C_s-symmetric transition state structures for their enantiomerizations.

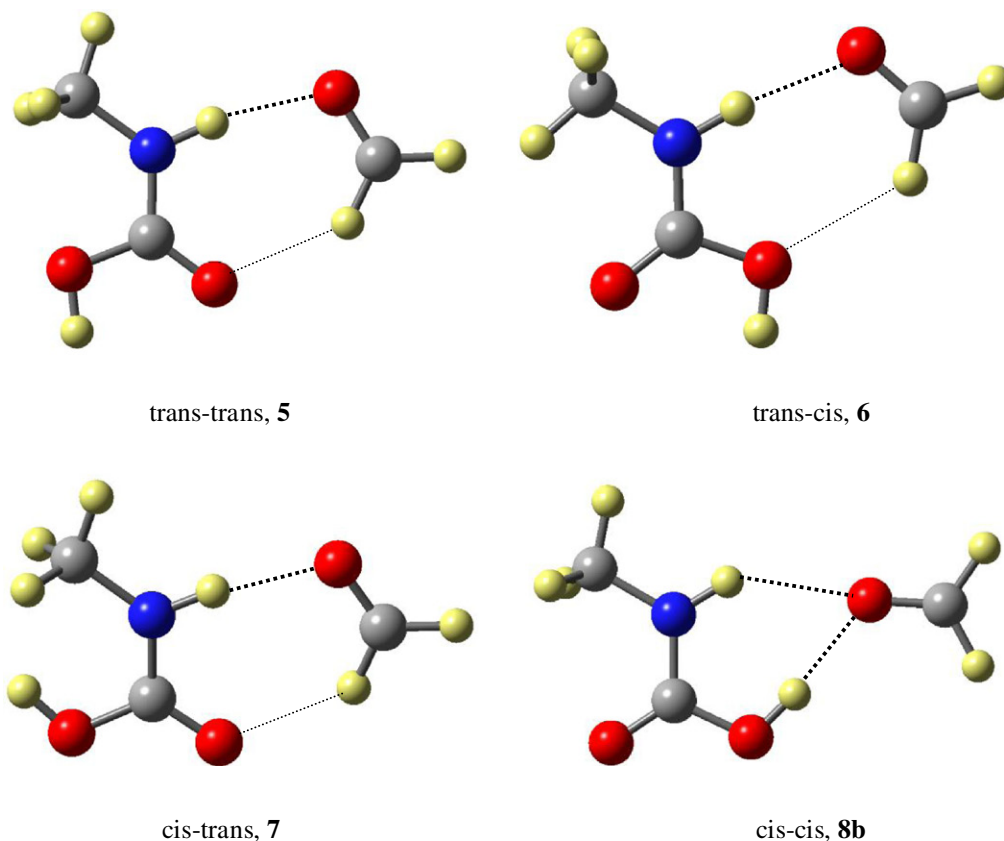


FIGURE 17.4 Molecular models of the optimized structures of aggregates formed between the stereoisomers of *N*-methylcarbamamic acid and model carbonyl compound formaldehyde. Major structural parameter (in Å and degrees) describing the intermolecular bonding situation: $d(\text{NH}\cdots\text{O})$: 1.986 (**5**), 2.015 (**6**), 1.967 (**7**), and 2.317 (**8b**); $d(\text{CO}\cdots\text{H})$: 2.278 (**5**), 2.458 (**6**), and 2.261 (**7**); and $d(\text{OH}\cdots\text{O})$: 1.920 (**8b**).

The aggregates **5** and **9b** of the trans-trans NMCA isomer **1** are the most relevant models in the present context. The trans-trans isomer of NMCA has the correct stereochemistry to simultaneously engage in hydrogen-bonding between its amide-H and the carbonyl binding site *and* in Mg^{2+} -complexation via its carbonyl-O (vide infra). Therefore, relative energies of the aggregates $\text{NMCA}\cdot(\text{A/K})$ reported in Table 17.2 are relative to **5** and **9b** (in spite of the fact that **10b** is slightly more stable than **9b**). The binding energies reported in Table 17.2 for the aggregates $\text{NMCA}\cdot(\text{A/K})$ all refer to the aggregation of a given NMCA isomer with retention of its stereochemistry.

The aggregates $\text{NMCA}\cdot(\text{A/K})$ generally feature a near-linear hydrogen-bond with the amide's N–H bond pointing toward one of the lone pair regions of the carbonyl compound and a secondary contact between a CH bond of the carbonyl and an acid-O (Figures 17.4–17.6). The cis-cis isomers of NMCA stand out in that they can engage in *two* hydrogen bonds with the carbonyl-O to form aggregates **8b** and **12b**, respectively. Nevertheless, the cis-cis isomers remain significantly less stable than any of the normal trans-acid isomers.

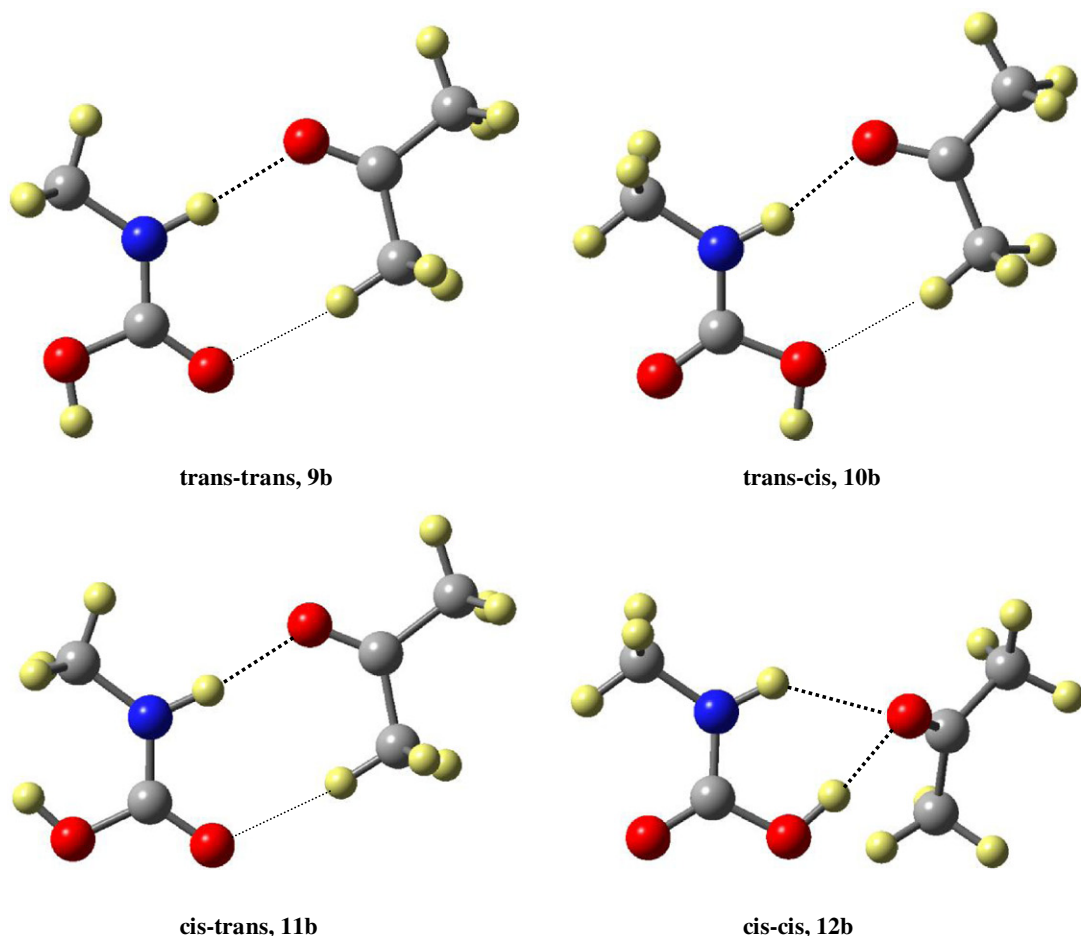


FIGURE 17.5 Molecular models of the optimized structures of aggregates formed between the stereoisomers of *N*-methylcarbaminic acid and model carbonyl compound acetone. Major structural parameter (in Å and degrees) describing the intermolecular bonding situation: $d(\text{NH}\cdots\text{O})$: 1.952 (**9b**), 1.993 (**10b**), 1.937 (**11b**), and 2.336 (**12b**); $d(\text{CO}\cdots\text{H}_{\text{Ac}})$: 2.314 (**9b**), 2.457 (**10b**), and 2.296 (**11b**); and $d(\text{OH}\cdots\text{O})$: 1.840 (**12b**).

The energies for the reactions R2a and R2b (Table 17.2) describe the aggregation of the previously free, independently moving and preferred NMCA trans-cis isomer **2** with formaldehyde (FA) or acetone (Ac), respectively, to form the trans-trans aggregates **5** and **9b**, respectively. With the thermochemical data for the aggregation reactions R3a and R3b, we can now evaluate the thermochemistry of the reaction R4a and R4b, that is, the additions of CO₂ to a carbonyl-aggregate of methylamine to form a carbonyl-aggregate of NMCA. The data in Table 17.2 show that carbonyl aggregation makes the NMCA formation about 3 kcal/mol more exothermic ($\Delta H(\text{R1}) = -2.0$ kcal/mol *vs.* $\Delta H(\text{R4a}) \approx \Delta H(\text{R4b}) = -4.8$ kcal/mol) and about 1 kcal/mol less endergonic ($\Delta G(\text{R1}) = +4.1$ kcal/mol *vs.* $\Delta G(\text{R4a}) \approx \Delta G(\text{R4b}) \approx 2.5-2.8$ kcal/

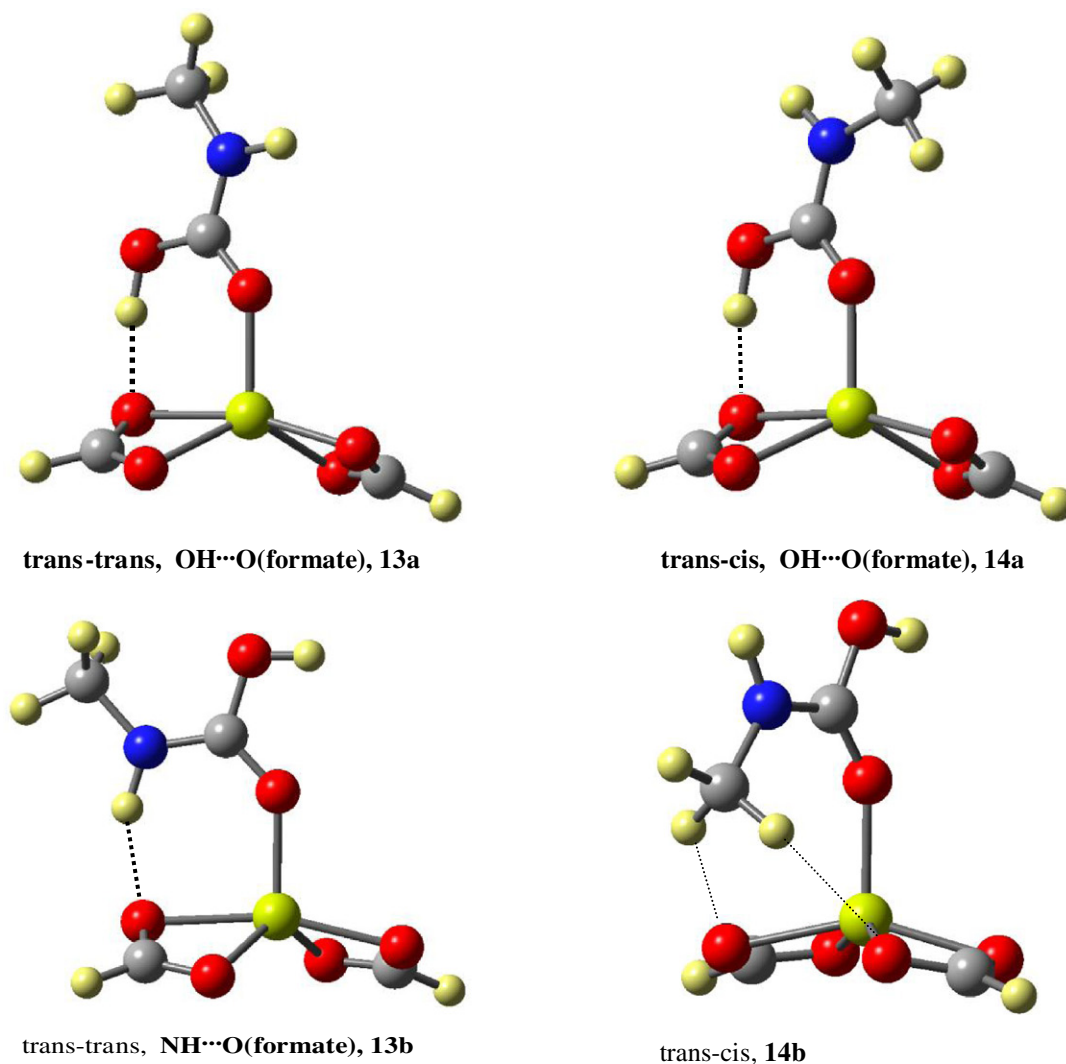


FIGURE 17.6 Molecular models of the optimized structures of complexes formed between the trans acid isomers of *N*-methylcarbamamic acid and magnesium formate. Major structural parameter (in Å and degrees) describing the intermolecular bonding situation: $d(\text{Mg}\cdots\text{O})$: 2.007 (13a), 2.020 (13b); 2.009 (14a), 2.022 (14b); $\angle(\text{Mg}-\text{O}-\text{C})$: 134.6 (13a), 134.6 (13b), 134.8 (14a), and 147.4 (4b); $d(\text{OH}\cdots\text{O})$: 1.659 (13a), 1.669 (14a); $d(\text{NH}\cdots\text{O})$: 1.864 (13b). In 14b, the *N*-methyl groups hydrogen atoms are pointed toward the proximate formate-O atoms: $d(\text{Me}-\text{H}\cdots\text{O})$: 2.501 and 2.510.

mol). While noticeable, the effect of carbonyl aggregation on the reaction thermochemistry is relatively small and, most importantly, this event still leaves the addition reaction thermodynamically unfavorable. It is the primary function of the carbonyl group in the rubisco active site (Asp202 or Asn192, see [Scheme 17.3](#)) to orient the substrates into proper conformations for reaction.

17.4.4 Magnesium Formate Complexes of *N*-Methylcarbaminoic Acid

We employ magnesium formate, MgL₂ (L = HCO₂⁻), to study Mg²⁺ complexation of NMCA in a small model system. We considered aggregates of magnesium formate formed with **1–4** and the optimized structures of the NMCA·MgL₂ systems are shown in [Figure 17.6](#) (trans-acid isomers) and [Figure 17.7](#) (cis-acid isomers).

All of the NMCA·MgL₂ aggregates feature Mg²⁺ coordination by the carbonyl-O of the NMCA molecule. The NMCA isomers with cis acid conformations were considered because of their potential to serve as bidentate ligands, that is, the potential that both the carbonyl-O and the acid's hydroxyl-O might coordinate simultaneously to the metal cation. However, the optimized structures show that this option is not realized and that only the NMCA's carbonyl-O coordinates to the Mg²⁺ ion. In addition to the primary $d(\text{Mg}\cdots\text{O}_{\text{NMCA}})$ contact, all of the NMCA·MgL₂ aggregates show secondary interactions between NMCA and the formate ligands. One of the NMCA's carbonyl σ -lone pairs coordinates to the Mg²⁺ ion and the nature of the secondary interaction depends on which carbonyl σ -lone pair engages in complex formation.

In isomers **13a** and **14a** ([Figure 17.6](#)), strong secondary interactions result from hydrogen-bonding between the trans acid's hydroxyl group and a formate-O with $d(\text{OH}\cdots\text{O})$ values of 1.659 Å (**13a**) and 1.669 Å (**14a**). In **13b** and **14b**, the NMCA's carbonyl coordinates the Mg²⁺ ion with its other lone pair and the *N*-methylamino group is placed in proximity to the formate ligands. Isomer **13b** benefits from a hydrogen-bonding interaction between NMCA's amide NH bond and a formate-O with $d(\text{NH}\cdots\text{O}) = 1.864$ Å. In **14b**, the *N*-methyl group's hydrogen atoms are pointed toward the proximate formate-O atoms ($d(\text{O}\cdots\text{H}_{\text{Me}})$: 2.501 and 2.510 Å) and there is some benefit from charge-induced polarization.

The coordination of NMCA isomers **3** and **4** with their cis acid moieties to magnesium formate results in the complexes **15** and **16** ([Figure 17.7](#)). With secondary OH \cdots O_{formate} hydrogen-bonding (as in **13a** and **14a**) no longer attainable, one formate-O instead approaches the next best electrophilic center: the NMCA's central carbon atom. The incipient nucleophilic attack interactions [72] are indicated by long-dash lines in [Figure 17.7](#), and the INA-distances are 3.133 Å (**15a**) and 3.149 Å (**16a**). The coordination modes of cis acid isomers **15b** and **16b** are similar to those in the trans acid isomers **13b** and **14b**, respectively.

The relative energies of the NMCA·MgL₂ complexes are given in [Table 17.2](#). Complex **14a** is the most stable structure and complex **13a** is a close second; both of the complexes feature η^1 -carbonyl coordination of Mg²⁺ together with an OH \cdots O_{formate} secondary contact. The isomer in **13a** with its additional OH \cdots O_{formate} contact is about 3.0 kcal/mol more stable isomer in **13b** with its additional NH \cdots O_{formate} contact. The absence of a secondary hydrogen-bonding contact in **14b** lowers the complex's stability by about 7 kcal/mol. All complexes of the cis acids **3** and **4** are less stable than **14a** by at least 10 kcal/mol. In the NMCA·MgL₂ complexes, the NMCA isomers with cis acid moieties do not benefit from bidentate coordination to Mg²⁺ cation and, to make things worse, they are destabilized by repulsion between the acid-OH and the carboxylate-Os.

The NMCA·MgL₂ complex formation energy describes the complexation of the most stable isomer of NMCA by magnesium formate leading to the formation of the most stable NMCA·MgL₂ complex: reaction **R5** is the reaction **2** + MgL₂ → **14a**. Reaction **R5** is exothermic by $\Delta H(\text{R5}) = -31.0$ kcal/mol and is exergonic by $\Delta G(\text{R5}) = -19.0$ kcal/mol ([Table 17.2](#)).

With the knowledge of the NMCA·MgL₂ complex formation energies, we are finally in a position to evaluate the thermochemistry of the NMCA formation reactions **R6** (no pre-coordination,

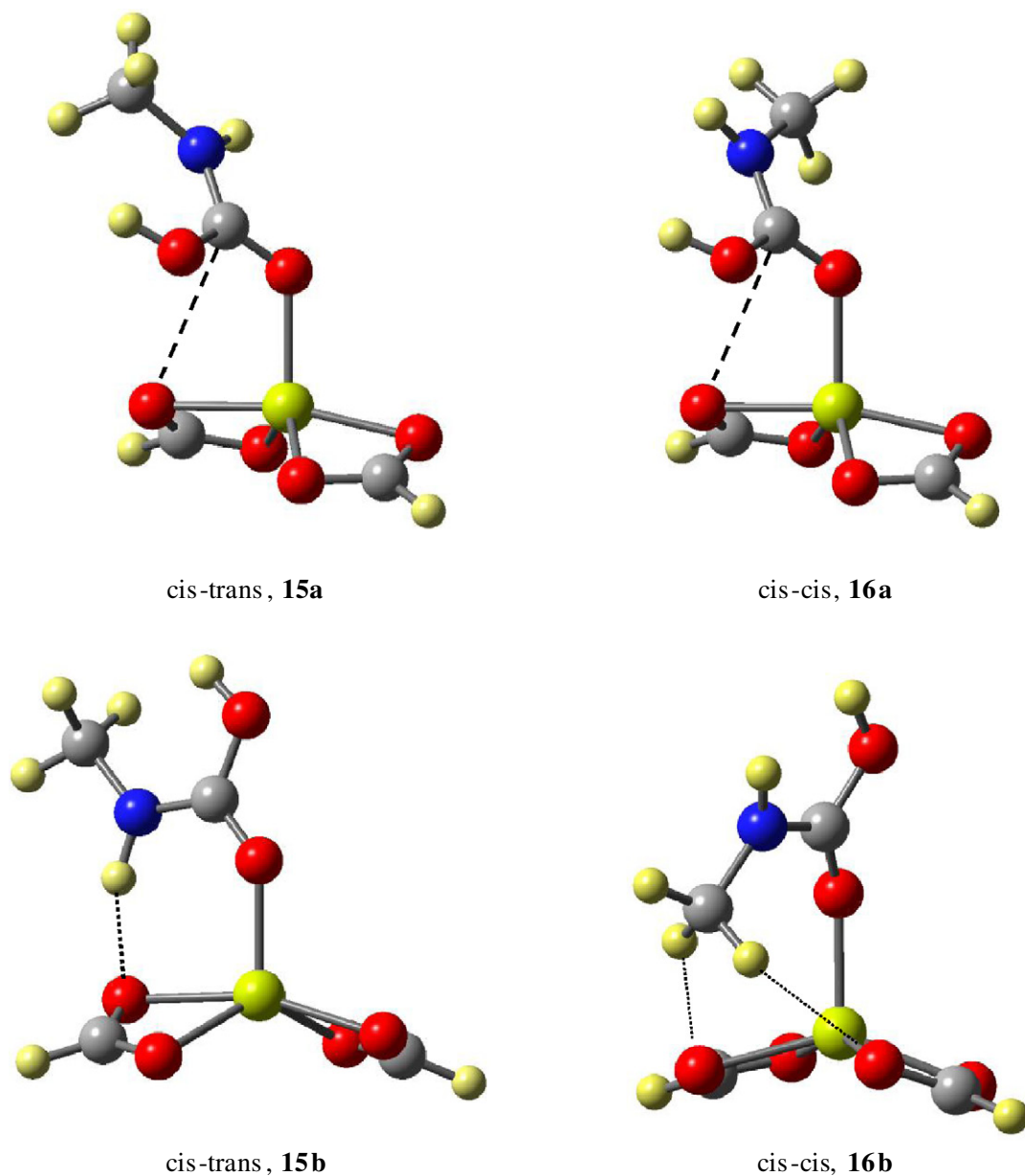


FIGURE 17.7 Molecular models of the optimized structures of complexes formed between the cis acid isomers of *N*-methylcarbamamic acid and magnesium formate. Major structural parameter (in Å and degrees) describing the intermolecular bonding situation: $d(\text{Mg}\cdots\text{O})$: 2.048 (**15a**), 2.015 (**15b**); 2.053 (**16a**), 2.018 (**16b**); $\angle(\text{Mg}-\text{O}-\text{C})$: 124.3 (**15a**), 135.3 (**15b**), 124.0 (**16a**), and 146.1 (**16b**); $d(\text{NH}\cdots\text{O})$: 1.864 (**15b**). Possible incipient nucleophilic attack interactions are indicated by long-dash lines and the INA-distances are 3.133 (**15a**) and 3.149 (**16a**). In **16b**, the *N*-methyl group's hydrogen atoms are pointed toward the proximate formate-O atoms: $d(\text{Me}-\text{H}\cdots\text{O})$: 2.539 and 2.448.

R6=R1+R5), R8 (CO₂·MgL₂ pre-coordination, R8=R6-R7), and R11 (H₂O·MgL₂ pre-coordination, R11=R8+R10). The most important computed results are $\Delta H(R6)=-33.0$ kcal/mol and $\Delta G(R6)=-15.0$ kcal/mol, $\Delta H(R8)=-28.7$ kcal/mol and $\Delta G(R8)=-15.2$ kcal/mol, and $\Delta H(R11)=-12.3$ kcal/mol and $\Delta G(R11)=-2.9$ kcal/mol (Table 17.2). These results allow for several important conclusions.

First, model systems that consider the effects of magnesium complexation show the Mg²⁺-catalyzed NMCA formation reaction to be exothermic and exergonic. Second, the Mg²⁺-catalyzed NMCA formation reactions R6 and R8 suggest a reaction enthalpy of about -30 ± 3 kcal/mol and a reaction free enthalpy of about -15 ± 1 kcal/mol. Third, both the exothermicity and the exergonicity of NMCA formation are significantly reduced when the water/CO₂ ligand exchange is accounted for in the Mg²⁺-catalyzed NMCA formation reaction R11. The NMCA formation reaction R11 is exergonic by just a few kcal/mol. Hence, it is the inclusion of the water/CO₂ ligand exchange in the Mg²⁺-catalyzed NMCA formation reaction R11 that produces a model for reversible NMCA formation, and we will elaborate in Section 17.4.6.

17.4.5 Carbonyl-Aggregates of Magnesium Formate Complexes of N-Methylcarbaminic Acid

The evaluation of “the full monty” model, that is, the NMCA formation reaction with simultaneous consideration of Mg²⁺-complexation and of carbonyl aggregation requires the knowledge of the structures and stabilities of the systems (A/K)·NMCA·MgL₂. A formal and complete approach would entail the determination of the structures of all isomers of (A/K)·NMCA·MgL₂ for each of the carbonyl compounds. However, in light of the insights gained from the analysis of the smaller systems, a more focused and limited exploration of the most relevant (A/K)·NMCA·MgL₂ systems should suffice. We explored the FA·NMCA·MgL₂ systems 17 of the trans-trans NMCA isomer 1 (FA·13, FA·1·MgL₂) and the systems 18 of the trans-cis NMCA isomer 2 (FA·14, FA·2·MgL₂). In light of the stabilities of complexes 15 and 16, the systems 19 (FA·15, FA·3·MgL₂) and 20 (FA·16, FA·4·MgL₂) were not studied. Finally, we explored only the most relevant Ac·NMCA·MgL₂ system 21, the system containing the trans-trans NMCA isomer 1 (Ac·13, Ac·1·MgL₂).

The structures of systems 17 and 18 are shown in Figures 17.8 and 17.9, respectively. Structures 17a and 17b are the expected FA adducts of structures 13a and 13b, respectively, and structure 17a is the most relevant model of the rubisco active site. Two stationary structures of system 21 are shown in Figure 17.10, and structure 21a is the model most relevant to the discussion of the active site of rubisco. Systems 17a and 21a are structurally similar and it is an advantage of the latter that contacts between carbonyl CH bonds and NMCA·MgL₂ are diminished.

The topologies of structures 13a and 13b are not retained in structures 17c–17f. Structures 17c and 17d can be seen as derivatives of 17a which result by insertion of FA into the OH···O_{formate} bond. Similarly, structures 17e and 17f can be seen as derivatives of 17b which result by insertion of FA into the NH···O_{formate} bond. There is little doubt that structures with these topologies also exist for model 21. The variety of the molecular topologies for 17 and 21 illustrates an important point about small molecule models in general. There is no doubt that small molecule models are attractive targets for theoretical study because of the reduction in the size of the computational task. At the same time, however, the independence of the molecular

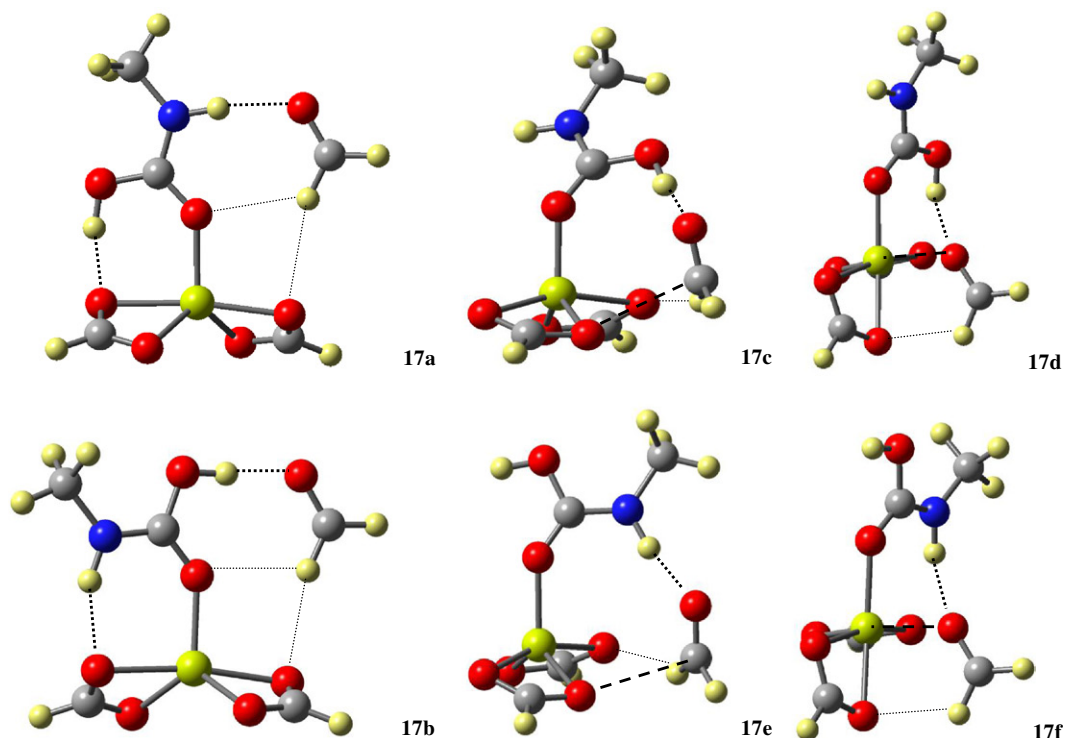


FIGURE 17.8 Stereoisomers of model aggregates **17** formed between the magnesium formate complexed trans-trans isomer of *N*-methylcarbaminc acid and model carbonyl formaldehyde (FA). Major structural parameter (in Å and degrees) describing the intermolecular bonding situation: $d(\text{Mg}\cdots\text{O})$: 1.988 (**17a**), 1.995 (**17b**); 1.987 (**17c**), 2.044 (**17d**), 1.998 (**17e**); 2.059 (**17f**); $\angle(\text{Mg}-\text{O}-\text{C})$: 136.3 (**17a**), 137.5 (**17b**); 140.5 (**17c**), 132.4 (**17d**), 141.6 (**17e**); 133.1 (**17f**); $d(\text{OH}\cdots\text{O})$: 1.710 (**17a**), 1.734 (**17b**), 1.679 (**17c**), 1.663 (**17d**); $d(\text{NH}\cdots\text{O})$: 1.936 (**17b**), 1.870 (**17e**), 1.877 (**17f**). In **17a** and **17b**, one formaldehyde H-atom also is in contact with the NMCA's carbonyl-O (**17a**: 2.547, **17b**: 2.504) and with a proximate formate-O (**17a**: 2.642, **17b**: 2.466). In **17c** and **17e**, the carbonyl engages in possible incipient nucleophilic (long-dash lines) with INA-distances of 2.676 (**17c**) and 2.801 (**17e**), and one of its H-atoms interacts with a formate-O (**17c**: 2.417; **17e**: 2.377). In **17d** and **17f**, the carbonyl compounds carbonyl-O atom coordinates Mg^{2+} (**17d**: 2.216; **17f**: 2.219) and one of its H-atoms interacts with a formate-O (**17d**: 2.285; **17f**: 2.284).

components (methylamine, carbonyl component, magnesium complex) of the small molecule model system increases the space of possible structural topologies. The palette of possible structural topologies in the active site geometry of a peptide is naturally limited by the structural constraints imposed by the peptide backbone on the relative positions of lysine, the carbonyl (amide-CO of Asp residue), and the (Asp, Glu)-ligated magnesium complex.

With the knowledge of the structures of the complexes (A/K)·NMCA·MgL₂, it is now possible to evaluate the thermochemistry of the NMCA formation reactions **R14**, $\text{H}_2\text{O}\cdot\text{MgL}_2 + \text{CO}_2 + \text{CH}_3\text{N H}_2\cdot(\text{A}/\text{K}) \rightarrow (\text{A}/\text{K})\cdot\text{NMCA}\cdot\text{MgL}_2 + \text{H}_2\text{O}$. The most important results for the formaldehyde model are $\Delta H(\text{R14a}) = -17.3$ kcal/mol and $\Delta G(\text{R14a}) = -6.6$ kcal/mol and for the acetone model they are $\Delta H(\text{R14b}) = -17.7$ kcal/mol and $\Delta G(\text{R14b}) = -5.5$ kcal/mol. The results are rather similar for both

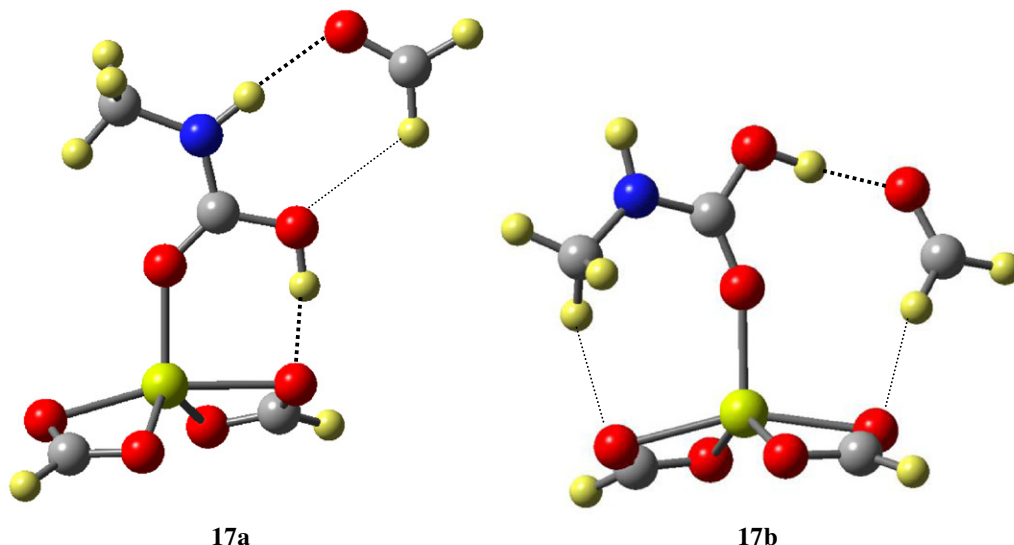


FIGURE 17.9 Stereoisomers of model aggregates **18** formed between the magnesium formate complexed trans-cis isomer of *N*-methylcarbaminoic acid and model carbonyl formaldehyde (FA). Major structural parameter (in Å and degrees) describing the intermolecular bonding situation: $d(\text{Mg}\cdots\text{O})$: 2.001 (**17a**), 1.990 (**17b**); $\angle(\text{Mg}-\text{O}-\text{C})$: 135.3 (**17a**), 158.4 (**17b**); $d(\text{OH}\cdots\text{O})$: 1.673 (**17a**), 1.714 (**17b**); $d(\text{NH}\cdots\text{O})$: 1.948 (**17a**). In **17b**, one of the *N*-methyl group's hydrogen atoms points toward the proximate formate-O atoms with $d(\text{Me}-\text{H}\cdots\text{O})=2.325$. Weak contacts between formaldehyde H-atom and proximate O-atoms (**17a**: 2.532, **17b**: 2.217).

carbonyl models in spite of the differences in the respective secondary interactions. Comparison of the thermochemistry of reaction **R14** ($\Delta H(\text{R14}) = -17.5 \pm 0.5 \text{ kcal/mol}$ and $\Delta G(\text{R14}) = -6 \pm 1 \text{ kcal/mol}$) to reaction **R11** ($\Delta H(\text{R11}) = -12.3 \text{ kcal/mol}$ and $\Delta G(\text{R11}) = -2.9 \text{ kcal/mol}$) suggests that the presence of the carbonyl binding site increases both the exothermicity and exergonicity of the NMCA formation.

17.4.6 Reversible *N*-Methylcarbaminoic Acid Formation and CO₂ Capture and Release

An exothermic ($\Delta H(T_1) < 0$) and exergonic ($\Delta G(T_1) < 0$) reaction with $\Delta H(T_1) < \Delta G(T_1)$ must have a negative reaction entropy $\Delta S(T_1)$ (i.e., $-T_1 \cdot \Delta S(T_1) > 0$). To reverse the reaction requires a perturbation of the system that raises $\Delta G(T_2)$ above zero. Assuming that the temperature dependences of ΔH and ΔS are negligible between temperatures T_1 and T_2 , at least to a first approximation, the reversal of the reaction would require a temperature increase $\Delta T = T_2 - T_1$ such that $\Delta T \cdot |\Delta S(T_1)| > |\Delta G(T_1)|$. The design of a system for reversible CO₂ capture thus requires a capture reaction with (1) a sufficiently negative reaction free enthalpy $\Delta G(T_1)$ to achieve effective capture, (2) a reaction free enthalpy $\Delta G(T_1)$ that is not too negative so that release is at all possible, and (3) a negative reaction entropy $\Delta S(T_1)$ of substantial magnitude so that CO₂ release can be achieved effectively with a moderate temperature increase.

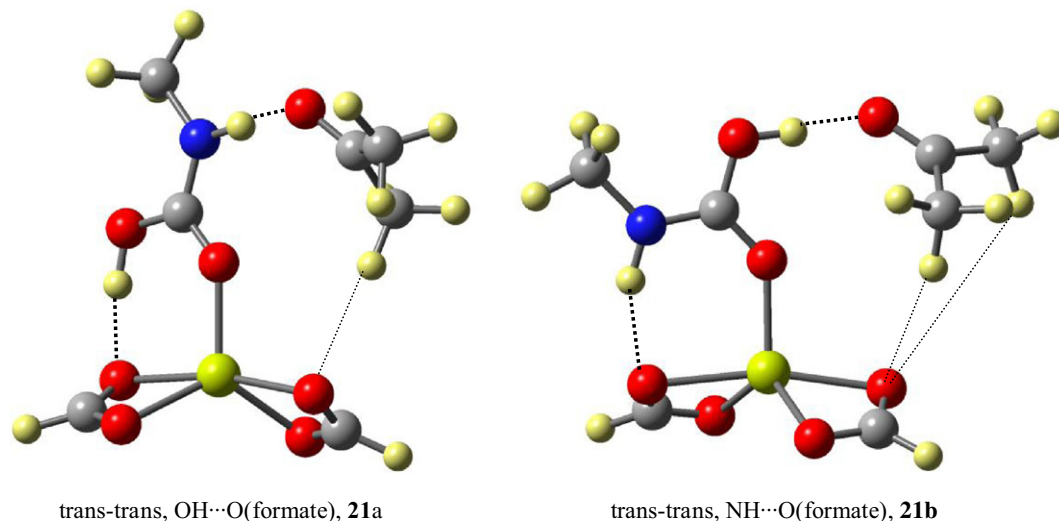


FIGURE 17.10 Stereoisomers of model aggregates **21** formed between the magnesium formate complexed trans-trans isomer of *N*-methylcarbaminic acid and model carbonyl acetone (Ac). Major structural parameter (in Å and degrees) describing the intermolecular bonding: $d(\text{Mg}\cdots\text{O})$: 1.985 (**21a**), 1.987 (**21b**); $\angle(\text{Mg}-\text{O}-\text{C})$: 136.2 (**21a**), 138.8 (**21b**); $d(\text{OH}\cdots\text{O})$: 1.711 (**21a**); $d(\text{NH}\cdots\text{O})$: 1.960 (**21b**). Weak contacts between acetone H-atom and proximate formate O-atoms (**21a**: 2.480, **21b**: 2.640, 2.705).

For the CO_2 capture reactions **R6** and **R8**, the $\Delta S(T_1)$ values are -60.8 and $-45.3 \text{ cal mol}^{-1} \text{ K}^{-1}$, respectively, and to achieve CO_2 release would require temperature increases ΔT of about 245° and 335° , respectively. With the water/ CO_2 ligand exchange reaction included, the $\Delta S(T_1)$ values of the CO_2 capture reactions **R11**, **R14a**, and **R14b** are -31.4 , -35.8 , and $-40.8 \text{ cal mol}^{-1} \text{ K}^{-1}$, respectively, and CO_2 release would require temperature increases ΔT of about 93° , 184° , and 136° , respectively.

The numerical examples illustrate well that one really has to pay attention to *all three* design criteria. It is not enough to focus on the overall reaction free enthalpy of the capture reaction and to design a weakly binding system that meets criteria (1) and (2). Instead, one wants to design a capture system that binds CO_2 with a large negative reaction enthalpy but *at an enormous cost in entropy*. For practical purposes, one wants to keep the temperature increase ΔT required for the release low and a goal of $\Delta T \approx 50\text{--}70^\circ$ would seem reasonable. For a capture reaction with $\Delta G(T_1) \approx -4 \text{ kcal/mol}$, meeting this ΔT target would require a capture system with $|\Delta S(T_1)| \approx 80\text{--}60 \text{ cal mol}^{-1} \text{ K}^{-1}$. To accomplish this design target will not be trivial because we have only a weak intuitive grasp of the entropy changes associated with binding events. The insights gained from the study of the small molecule models of the rubisco active site present an excellent starting point for systematic studies of functional and practical CO_2 capture systems. We are confident that rubisco-inspired biomimetic CO_2 capture systems can be developed using rational strategies based on in-depth studies of reaction thermochemistry.

17.5 CONCLUSION AND OUTLOOK

We described an approach for the reversible CO₂ capture from air based on the enzyme mechanism of the rubisco-catalyzed biological CO₂ fixation. The design of the rubisco-inspired biomimetic systems is informed by the understanding of the binding of the activator CO₂, ^ACO₂, in rubisco. The activation of rubisco involves the carbamylation of lysine and this CO₂ capture by lysine is likely to benefit from Mg²⁺-complexation and from hydrogen-bonding between the carbamate's amide-H and the active site aspartic acid (or asparagine).

We explored the carbamylation reaction in the rubisco active site with several small molecule models of *N*-methylcarbaminic acid (NMCA) formation in the presence of a simple carbonyl compound (aldehyde or ketone) and with magnesium formate as a simple model of the Mg²⁺ receptor site. The Mg²⁺-catalyzed formation of carbonyl-aggregates of NMCA is rather exothermic and exergonic, and it is only for the thermochemistry of the water/CO₂ ligand exchange reaction at the Mg²⁺ site that the reversal of NMCA formation becomes possible. We determined reaction energies of $\Delta H(\text{R14}) = -17.5 \pm 0.5 \text{ kcal/mol}$ and $\Delta G(\text{R14}) = -6 \pm 1 \text{ kcal/mol}$ for our best model, reaction R14: $\text{H}_2\text{O} \cdot \text{MgL}_2 + \text{CO}_2 + \text{CH}_3\text{NH}_2 \cdot (\text{A/K}) \rightarrow (\text{A/K}) \cdot \text{NMCA} \cdot \text{MgL}_2 + \text{H}_2\text{O}$. The discussion of the thermochemistry of the CO₂ capture reaction ($\Delta H(T_1) < \Delta G(T_1) < 0$) and of the condition for CO₂ release upon an increase in temperature ($|\Delta T \cdot |\Delta S(T_1)|| > |\Delta G(T_1)|$) shows the need for the development of CO₂ capture reactions with negative reaction entropies $\Delta S(T_1)$ of substantial magnitude ($|\Delta S(T_1)| \approx 80 - 60 \text{ cal mol}^{-1} \text{ K}^{-1}$).

We studied the system {CO₂, CH₃NH₂, (A/K), MgL₂} and there are many possibilities for refinements by way of exploration of the more general systems {CO₂, R-NH₂, O=CR¹R², (H₂O)_{*n*}MgL¹L²}. What are the effects of the nature of the alkylamine RNH₂ on the reaction thermochemistry? What are the thermochemical effects of using an amide as hydrogen-bond accepting carbonyl compound? And most importantly, how does the reaction thermochemistry depend on the nature of the Mg²⁺ complex? The structures of the systems NMCA·MgL₂ and (A/K)·NMCA·MgL₂ all showed secondary interactions involving the formate-O atoms, and these interactions will differ for models with other magnesium salts. More generally, we anticipate a tremendous potential for system modulation via modification of the Mg²⁺ site. The simple MgL₂ moiety used in the present study, magnesium formate, served as a good starting point to understand the competition between water, CO₂, and NMCA for the metal site. At the next level of sophistication, one needs to explore refined systems with Mg²⁺ sites that feature, for example, two monodentate carboxylates, more water molecules, and higher coordination numbers.

In the small molecule model system {CO₂, CH₃NH₂, (A/K), MgL₂} the four components were treated as independent. In the rubisco active site, on the other hand, three of the components are part of the protein chain and the primary amino group, the hydrogen-bond acceptor carbonyl (HBAC), and the magnesium complex (MC) are separated by spacers [S1] and [S2]; i.e., the linked system {CO₂, H₂N-[S1]-(HBAC)-[S2]-(MC)}. It will be interesting to explore the thermochemical consequences of linking the three components together. As a first step in that direction we are currently exploring small peptide models of the rubisco active site (CH₃O-Lys-Asp-Asp-Glu-NH₂, CH₃O-Lys-Gly-Asp-Glu-NH₂) both with computational and experimental methods.

SUPPLEMENTRY DATA

Cartesian coordinates of all stationary structures are available online (21 pages). The materials also can be obtained directly from the author.

References

- [1] R.F. Keeling, Recording Earth's vital signs, *Science* 319 (2008) 1771–1772.
- [2] Trends in Atmospheric Carbon Dioxide, US Department of Commerce, National Oceanic & Atmospheric Administration (NOAA), Earth System Research Laboratory, Global Monitoring Division. <<http://www.esrl.noaa.gov/gmd/ccgg/trends>> (accessed 01.15.13).
- [3] CarbonTracker, US Department of Commerce, National Oceanic & Atmospheric Administration (NOAA), Earth System Research Laboratory, Global Monitoring Division. <<http://www.esrl.noaa.gov/gmd/ccgg/carbon-tracker>> (accessed 01.15.13).
- [4] W. Peters, A.R. Jacobson, C. Sweeney, A.E. Andrews, T.J. Conway, K. Masarie, J.B. Miller, L.M.P. Bruhwiler, G. Pétron, A.I. Hirsch, D.E.J. Worthy, G.R. van der Werf, J.T. Randerson, P.O. Wennberg, M.C. Krol, P.P. Tans, An atmospheric perspective on North American carbon dioxide exchange: CarbonTracker, *Proc. Natl. Acad. Sci.* 104 (2007) 18925–18930.
- [5] United States Carbon Cycle Science Program. <<http://www.carboncyclescience.gov>> (accessed 01.15.13).
- [6] A.W. King, L. Dilling, G.P. Zimmerman, D.M. Fairman, R.A. Houghton, G.A. Marland, A.Z. Rose, T.J. Willbanks (Eds.), *The First State of the Carbon Cycle Report (SOCCR). The North American Carbon Budget and Implications for the Global Carbon Cycle*, US Climate Change Science Program, Washington, DC, November 13, 2007.
- [7] A.M. Michalak, R.B. Jackson, G. Marland, C. Sabine, the Carbon Cycle Science Working Group, A US Carbon Cycle Science Plan, US Climate Change Science Program, Washington, DC, August 2011. <<http://www.carboncyclescience.gov/USCarbonCycleSciencePlan-August2011.pdf>> (accessed 01.15.13).
- [8] OCO-2, Orbiting Carbon Observatory, NASA, Jet Propulsion Laboratory. <<http://oco.jpl.nasa.gov>> (accessed 01.15.13).
- [9] Intergovernmental Panel on Climate Change (IPCC). <<http://www.ipcc.ch>> (accessed 01.15.13).
- [10] IPCC Fourth Assessment Report: Climate Change 2007 (AR4). <http://www.ipcc.ch/publications_and_data/publication_and_data_reports.shtml#1> (accessed 01.15.13).
- [11] (a) F.C. Moore, Carbon Dioxide Emissions Accelerating Rapidly, Earth Policy Institute, Washington, DC, April 9, 2008. <http://www.earth-policy.org/indicators/C52/carbon_emissions_2008> (accessed 01.15.13). (b) World Carbon Dioxide Emissions from Fossil Fuel Combustion in 2006 and 2008, with IEA Projection for 2020, January 12, 2011. <http://www.earth-policy.org/data_center/C23> (accessed 01.15.13).
- [12] Global Carbon Project. <<http://www.globalcarbonproject.org>> (accessed 01.15.13).
- [13] Carbon Budget 2012. Global Carbon Project, December 12, 2012. <<http://www.globalcarbonproject.org/carbonbudget>> (accessed 01.15.13).
- [14] (a) A. Gore, *An Inconvenient Truth: The Planetary Emergency of Global Warming and What We Can Do About It*. Rodale Books, 2006. (b) Alliance for Climate Protection. <<http://www.wecansolveit.org>> (accessed 01.15.13). (c) J. Eilperin, Gore Launches Ambitious Advocacy Campaign on Climate, *The Washington Post*, March 31, 2008.
- [15] The Carbon Bathtub. *National Geographic Magazine*, 2009. <<http://ngm.nationalgeographic.com/big-idea/05/carbon-bath>> (accessed 01.15.13).
- [16] (a) D.G. Victor, *The collapse of the Kyoto protocol and the struggle to slow global warming*, Princeton University Press, 2004; (b) W.T. Douma, L. Massai, M. Montini, *The Kyoto Protocol and beyond: legal and policy challenges of climate change*, Asser Press, 2007.
- [17] R.E. Hester, R.M. Harrison (Eds.), *Carbon capture and storage, Issues in Environmental Science and Technology*, vol. 25, RSC Publishing: Royal Society of Chemistry, Cambridge, UK, 2010.
- [18] J. Wilcox, *Carbon Capture*, Springer, New York, 2012.
- [19] R. Guerrero-Lemus, J.M. Martínez-Duart, *Renewable energies and CO₂—Cost analysis, environmental impacts and technological trends—2012 edition*, *Lecture Notes in Energy*, vol. 3, Springer, New York, 2013.
- [20] P. Folger, *Carbon Capture and Sequestration: Research, Development, and Demonstration at the US Department of Energy*, CreateSpace Independent Publishing Platform, 2012.

- [21] J.F.P. Gomes (Ed.), *Carbon Dioxide Capture and Sequestration: An Integrated Overview of Available Technologies*, Nova Science Publishers, Inc., Hauppauge, New York, 2013.
- [22] W. Cao, D. Zheng, Thermodynamic performance of O₂/CO₂ gas turbine cycle with chemical recuperation by CO₂-reforming of methane, *Fuel* 86 (2007) 2864–2870.
- [23] (a) Powerspan—Clean Energy Technology. <<http://powerspan.com>> (accessed 01.15.13). (b) ECO₂ Technology. <<http://powerspan.com/technology/eco2-co2-capture>> (accessed 01.15.13).
- [24] (a) Alstom—Carbon capture and Storage. <<http://www.alstom.com/power/coal-oil/carbon-capture-solutions/>> (accessed 01.15.13). (b) R. Peltier, Carbon capture: Alstom's chilled ammonia CO₂-capture process advances toward commercialization, *Power* 152 (2008) 38.
- [25] R.P. Lively, R.R. Chance, W.J. Koros, Enabling low-cost CO₂ capture via heat integration, *Ind. Eng. Chem. Res.* 49 (2010) 7550–7562.
- [26] (a) J.T. Yeh, K.P. Resnik, K. Rygle, H.W. Pennline, Semi-batch absorption and regeneration studies for CO₂ capture by aqueous ammonia, *Fuel Processing Techn.* 86 (2005) 1533–1546; (b) F.A. Tobiesen, H.F. Svendsen, T. Mejdell, Modeling of blast furnace CO₂ capture using amine absorbents, *Ind. Eng. Chem. Res.* 46 (2007) 7811–7819; (c) Z. Sun, M. Fan, M. Argyle, Supported monoethanolamine for CO₂ separation, *Ind. Eng. Chem. Res.* 50 (2011) 11343–11349.
- [27] (a) J. Kuntz, A. Aronwilas, Performance of spray column for CO₂ capture application, *Ind. Eng. Chem. Res.* 47 (2008) 145–153; (b) M.R.M. Abu-Zahra, J.P.M. Niederer, P.H.M. Feron, G.F. Versteeg, CO₂ capture from power plants part II. A parametric study of the economical performance based on mono-ethanolamine, *Int J Green Gas Cont* 1 (2007) 135–142.
- [28] R. Idem, M. Wilson, P. Tontiwachwuthikul, A. Chakma, A. Veawab, A. Aronwilas, D. Gelowitz, Pilot plant studies of the CO₂ capture performance of aqueous MEA and mixed MEA/MDEA solvents at the University of Regina CO₂ capture technology development plant and the Boundary Dam CO₂ capture demonstration plant, *Ind. Eng. Chem. Res.* 45 (2006) 2414–2420.
- [29] F.S. Zeman, K.S. Lackner, Capturing carbon dioxide directly from the atmosphere, *World Resources Rev.* 16 (2004) 62–68.
- [30] K.S. Lackner, S. Brennan, Envisioning carbon capture and storage: expanded possibilities due to air capture, leakage insurance, and C-14 monitoring, *Clim. Change* 96 (2009) 357–378.
- [31] First Successful Demonstration of Carbon Dioxide Air Capture Technology Achieved. By Earth Institute at Columbia University, posted at physorg.com April 25, 2007. <<http://www.physorg.com/news96732819.html>> (accessed 01.22.13).
- [32] R. Kunzig, Mopping up the CO₂ deluge, *Time Mag.* 172 (2008) 40–43 (July 14).
- [33] D.W. Keith, M. Ha-Duong, J.K. Stolaroff, Climate strategy with CO₂ capture from the air, *Clim. Change* 74 (2006) 17–45.
- [34] R. Socolow, M. Desmond, R. Aines, J. Blackstock, O. Bolland, T. Kaarsberg, N. Lewis, M. Mazzotti, A. Pfeffer, K. Sawyer, J. Sirola, B. Smit, J. Wilcox, Direct Air Capture of CO₂ with Chemicals: A Technology Assessment for the APS Panel on Public Affairs. (American Physical Society, 2011) . <<http://www.aps.org/policy/reports/assessments/upload/dac2011.pdf>> (accessed 01.15.13).
- [35] M. Lavelle, Out of thin air: the quest to capture carbon dioxide, *Natl. Geogr. Mag.* 2011. <<http://news.national-geographic.com/news/energy/2011/08/110811-quest-to-capture-carbon-dioxide/>> (accessed 01.15.13).
- [36] A. Goepfert, M. Czaun, R.B. May, G.K.S. Prakash, G.A. Olah, S.R. Narayanan, Carbon dioxide capture from the air using a polyamine based regenerable solid adsorbent, *J. Am. Chem. Soc.* 133 (2011) 20164–20167.
- [37] T. McDonald, W.R. Lee, J.A. Mason, B.M. Wiers, C.S. Hong, J.R. Long, Capture of carbon dioxide from air and flue gas in the alkylamine-appended metal-organic framework mmen-Mg₂(dobpdc), *J. Am. Chem. Soc.* 134 (2012) 7056–7065.
- [38] K. Sumida, D.L. Rogow, J.A. Mason, T.M. McDonald, E.D. Bloch, Z.R. Herm, T.-H. Bae, J.R. Long, Carbon dioxide capture in metal-organic frameworks, *Chem. Rev.* 112 (2012) 724–781.
- [39] R. Poloni, B. Smit, J.B. Neaton, Ligand-assisted enhancement of CO₂ capture in metal-organic frameworks, *J. Am. Chem. Soc.* 134 (2012) 6714–6719.
- [40] Z.-Z. Yang, Q.-W. Song, L.-N. He, *Capture and Utilization of Carbon Dioxide with Poly-Ethylene Glycol*, SpringerBriefs in Molecular Science, Springer, New York, 2012.
- [41] L. Li, M.-L. Fu, Y.-H. Zhao, Y.-T. Zhu, Characterization of carbonic anhydrase II from *Chlorella vulgaris* in bio-CO₂ capture, *Environ. Sci. Pollut. Res.* 19 (2012) 4227–4232.
- [42] R. Glaser, Z. Wu, M. Lewis, A higher level ab initio quantum-mechanical study of the quadrupole moment tensor components of carbon dioxide, *J. Mol. Struct.* 556 (2000) 131–141.

- [43] R. Glaser, M. Lewis, Z. Wu, Theoretical study of the quadrupolarity of carbodiimide, *J. Phys. Chem. A* 106 (2002) 7950–7957.
- [44] M. Lewis, Z. Wu, R. Glaser, Polarizabilities of carbon dioxide and carbodiimide. Assessment of theoretical model dependencies on dipole polarizabilities and dipole polarizability anisotropies, *J. Phys. Chem. A* 104 (2000) 11355–11361.
- [45] M. Lewis, R. Glaser, Synergism of catalysis and reaction center rehybridization. A novel mode of catalysis in the hydrolysis of carbon dioxide, *J. Phys. Chem. A* 107 (2003) 6814–6818.
- [46] M. Lewis, R. Glaser, Synergism of catalysis and reaction center rehybridization. An ab initio study of the hydrolysis of the parent carbodiimide, *J. Am. Chem. Soc.* 120 (1998) 8541–8542.
- [47] M. Lewis, R. Glaser, Synergism of catalysis and reaction center rehybridization in nucleophilic additions to cumulenes: the one-, two- and three-water hydrolyses of carbodiimide and methyleneimine, *Chem. Eur. J.* 8 (2002) 1934–1944.
- [48] J.M. Shively, G. Van Keulen, W.G. Meijer, Something about almost nothing: CO₂ fixation in chemototrophs, *Ann. Rev. Microbiol.* 52 (1998) 191–230.
- [49] B. Kusian, B. Bowien, Organization and regulation of cbb CO₂ assimilation genes in autotrophic bacter, *FEMS Microbiol. Rev.* 21 (1997) 135–155.
- [50] M. Hugler, S.M. Sievert, Beyond the Calvin cycle: autotrophic carbon fixation in the ocean, *Ann. Rev. Marine Sci.* 3 (2011) 89–261.
- [51] O. Mueller-Cajar, M.R. Badger, New roads lead to Rubisco in archaeobacteria, *BioEssays* 29 (2007) 722–724.
- [52] PDB 1AUS (a) T.C. Taylor, I. Andersson, Structure of a product complex of spinach ribulose-1,5-bisphosphate carboxylase/oxygenase, *Biochemistry* 36 (1997) 4041–4046; (b) T.C. Taylor, I. Andersson, Structural transitions during activation and ligand binding in hexadecameric Rubisco inferred from the crystal structure of the activated unliganded spinach enzyme, *Nat. Struct. Biol.* 3 (1996) 95–101.
- [53] S. Gutteridge, J. Newman, C. Herrmann, D. Rhoades, The crystal structures of Rubisco and opportunities for manipulating photosynthesis, *J. Exp. Botany* 46 (1995) 1261–1267.
- [54] PDB 2RUS T. Schneider, G. Crystal, Structure of the ternary complex of ribulose-1,5-bisphosphate carboxylase, magnesium(II) and activator carbon dioxide at 2.3 Å resolution, *Biochemistry* 30 (1991) 904–908.
- [55] PDB 1WDD H. Matsumura, E. Mizohata, H. Ishida, A. Kogami, T. Ueno, A. Makino, T. Inoue, A. Yokota, T. Mae, Y. Kai, Crystal structure of rice Rubisco and implications for activation induced by positive effectors NADPH and 6-phosphogluconate, *J Mol Biol.* 422 (2012) 75–86.
- [56] PDB 1GK8 (a) T.C. Taylor, A. Backlund, K. Bjorhall, R.J. Spreitzer, I. Andersson, First crystal structure of Rubisco from a green alga, *Chlamydomonas reinhardtii*, *J. Biol. Chem.* 276 (2001) 48159–48164; PDB 1IIR1: (b) E. Mizohata, H. Matsumura, Y. Okano, M. Kumei, H. Takuma, J. Onodera, K. Kato, N. Shibata, T. Inoue, A. Yokota, Y. Kai, Crystal structure of activated ribulose-1,5-bisphosphate carboxylase/oxygenase from green alga *Chlamydomonas reinhardtii* complexed with 2-carboxyarabinitol-1,5-bisphosphate, *J Mol Biol.* 316 (2002) 679–691.
- [57] M. Baranowski, B. Stec, Crystallization and characterization of *Galdieria sulphuraria* RUBISCO in two crystal forms: structural phase transition observed in P21 crystal form, *Intl. J. Mol. Sci.* 8 (2007) 1039–1051.
- [58] A.P. Duff, T.J. Andrews, P.M.G. Curmi, The transition between the open and closed states of rubisco is triggered by the interphosphate distance of the bound bisphosphate, *J. Mol. Biol.* 298 (2000) 903–916.
- [59] (a) F.C. Hartman, M.R. Harpel, Structure, function, regulation, and assembly of D-ribulose-1,5-bisphosphate carboxylase/oxygenase, *Annu. Rev. Biochem.* 63 (1994) 197–234; (b) W.W. Cleland, T.J. Andrews, S. Gutteridge, F.C. Hartman, G.H. Lorimer, Mechanism of Rubisco: the carbamate as general base, *Chem. Rev.* 98 (1998) 549–561; (c) R.J. Spreitzer, M.E. Salvucci, Rubisco: structure, regulatory interactions, and possibilities for a better enzyme, *Ann. Rev. Plant. Biol.* 53 (2002) 449–475.
- [60] (a) A.E. Portis, M.E. Salvucci, The discovery of Rubisco activase—yet another story of serendipity, *Photosynthesis Res.* 73 (2002) 257–264; (b) A.R. Portis, C. Li, D. Wang, M.E. Salvucci, Regulation of Rubisco activase and its interaction with Rubisco, *J. Exp. Botany* 59 (2008) 1597–1604.
- [61] (a) O. Tapia, H. Fidder, V.S. Safont, M. Oliva, J. Andrés, Enzyme catalysis: transition structures and quantum dynamical aspects: modeling Rubisco's oxygenation and carboxylation mechanisms, *Intl. J. Quant. Chem.* 88 (2002) 154–166; (b) M. Oliva, V.S. Safont, J. Andres, O. Tapia, Transition structures for D-Ribulose-1,5-bisphosphate carboxylase/oxygenase-catalyzed oxygenation chemistry: role of carbamylated lysine in a model magnesium coordination sphere, *J. Phys. Chem. A* 105 (2001) 4726–4736; (c) O. Tapia, M. Oliva, V.S. Safont, J. Andres, A quantum-chemical study of transition structures for enolization and oxygenation steps catalyzed by Rubisco: on the role of magnesium and carbamylated Lys-201 in opening oxygen capture channel, *Chem. Phys.*

- Lett. 323 (2000) 29–34; (d) M. Oliva, V.S. Safont, J. Andres, O. Tapia, Theoretical study of the molecular mechanism for the oxygenation chemistry in Rubisco, *J. Phys. Chem. A* 103 (1999) 6009–6016.
- [62] (a) S. Gutteridge, J. Pierce, A unified theory for the basis of the limitations of the primary reaction of photosynthetic CO₂ fixation: was Dr. Pangloss right? *Proc. Natl. Acad. Sci. USA* 103 (2006) 7203–7204; (b) G.G.B. Tcherkez, G.D. Farquhar, T.J. Andrews, *Proc. Natl. Acad. Sci. USA* 103 (2006) 7246–7251.
- [63] G.A. Olah, Towards oil independence through renewable methanol chemistry, *Angew. Chem. Int. Ed.* 52 (2013) 104–107.
- [64] A. Ambrosini, E.N. Coker, M.A. Rodriguez, S. Livers, L.R. Evans, J.E. Miller, E.B. Stechel, Synthesis and characterization of ferrite materials for thermochemical CO₂ splitting using concentrated solar energy, advances in CO₂ conversion and utilization, in: Y. Hu (Ed.), *ACS Symposium Series*, American Chemical Society, Washington, DC, 2010 (Chapter 1).
- [65] (a) P. Furler, J. Scheffe, M. Gorbar, L. Moes, U. Vogt, A. Steinfeld, Solar thermochemical CO₂ splitting utilizing a reticulated porous ceria redox system, *Energy Fuels* 26 (2012) 7051–7059; (b) P.G. Loutzenhiser, M.E. Galvez, I. Hischier, A. Stamatou, A. Frei, A. Steinfeld, CO₂ splitting via two-step solar thermochemical cycles with Zn/ZnO and FeO/Fe₃O₄ redox reactions II: kinetic analysis, *Energy Fuels* 23 (2009) 2832–2839.
- [66] C.J. Cramer, *Essentials of Computational Chemistry*, Wiley, New York, NY, 2004.
- [67] (a) W. Koch, M.C. Holthausen, *A Chemist's Guide to Density Functional Theory*, second ed., Wiley-VCH, Weinheim, 2001; (b) D. Sholl, J.A. Steckel, *Density Functional Theory: A Practical Introduction*, first ed., Wiley-Interscience, New York, 2009.
- [68] A.D. Becke, Density-functional thermochemistry. III. The role of exact exchange, *J. Chem. Phys.* 98 (1993) 5648–5652.
- [69] (a) R. Ditchfield, W.J. Hehre, J.A. Pople, Self-consistent molecular orbital methods. 9. Extended Gaussian-type basis for molecular-orbital studies of organic molecules, *J. Chem. Phys.* 54 (1971) 724–728; (b) W.J. Hehre, R. Ditchfield, J.A. Pople, Self-consistent molecular orbital methods. 12. Further extensions of Gaussian-type basis sets for use in molecular-orbital studies of organic-molecules, *J. Chem. Phys.* 56 (1972) 2257–2261; (c) P.C. Hariharan, J.A. Pople, Influence of polarization functions on molecular-orbital hydrogenation energies, *Theor. Chem. Acc.* 28 (1973) 213–222; (d) M.M. Francl, W.J. Pietro, W.J. Hehre, J.S. Binkley, D.J. DeFrees, J.A. Pople, M.S. Gordon, Self-consistent molecular orbital methods. 23. A polarization-type basis set for 2nd-row elements, *J. Chem. Phys.* 77 (1982) 3654–3665.
- [70] M.J. Frisch, G.W. Trucks, H.B. Schlegel, G.E. Scuseria, M.A. Robb, J.R. Cheeseman, G. Scalmani, V. Barone, B. Mennucci, G.A. Petersson, H. Nakatsuji, M. Caricato, X. Li, H.P. Hratchian, A.F. Izmaylov, J. Bloino, G. Zheng, J.L. Sonnenberg, M. Hada, M. Ehara, K. Toyota, R. Fukuda, J. Hasegawa, M. Ishida, T. Nakajima, Y. Honda, O. Kitao, H. Nakai, T. Vreven, J.A. Montgomery Jr., J.E. Peralta, F. Ogliaro, M. Bearpark, J.J. Heyd, E. Brothers, K.N. Kudin, V.N. Staroverov, T. Keith, R. Kobayashi, J. Normand, K. Raghavachari, A. Rendell, J.C. Burant, S.S. Iyengar, J. Tomasi, M. Cossi, N. Rega, J.M. Millam, M. Klene, J.E. Knox, J.B. Cross, V. Bakken, C. Adamo, J. Jaramillo, R. Gomperts, R.E. Stratmann, O. Yazyev, A.J. Austin, R. Cammi, C. Pomelli, J.W. Ochterski, R.L. Martin, K. Morokuma, V.G. Zakrzewski, G.A. Voth, P. Salvador, J.J. Dannenberg, S. Dapprich, A.D. Daniels, O. Farkas, J.B. Foresman, J.V. Ortiz, J. Cioslowski, D.J. Fox, *Gaussian 09, Rev. B.01*, Gaussian, Inc., Wallingford, CT, 1994.
- [71] R. Dennington, T. Keith, J. Millam, *GaussView 5.0.8*, Semicem Inc., Shawnee Mission, KS, 2009.
- [72] (a) R. Glaser, C. Horan, E. Nelson, M.K. Hall, Incipient nucleophilic attack as a probe for the electronic structure of diazonium ions. An analysis of neighboring group interactions in β-carboxyvinylidiazonium ions, *J. Org. Chem.* 57 (1992) 215–228; (b) C.J. Horan, C.L. Barnes, R. Glaser, 2-carboxybenzenediazonium chloride monohydrate, *Acta Cryst. C* 49 (1993) 507–509; (c) C.J. Horan, P.E. Haney, C.L. Barnes, R. Glaser, Symmetrically H-bridged dimer of 2-carboxylatobenzenediazonium. The 1:1 complex between 2-carboxybenzenediazonium chloride and 2-carboxylatodiazonium Zwitterion, *Acta Cryst. C* 49 (1993) 1525–1528; (d) C.J. Horan, C.L. Barnes, R. Glaser, Crystal structure of the explosive parent benzyne precursor: 2-carboxylatobenzenediazonium hydrate, *Chem. Ber.* 126 (1993) 243–249; R. Glaser, C.J. Horan, Interpretation of neighboring group interactions in crystal structures. A solid state and quantum-chemical study of incipient nucleophilic attack in 2-diazonium benzoic acid and its benzoate, *Can. J. Chem.* 74 (1996) 1200–1214.
- [73] J. Andres, V. Moliner, J. Krechl, E. Silla, A theoretical study of the addition mechanism of carbon dioxide to methylamine. Modelling CO₂-biotin fixation, *J. Chem. Soc. Perkin Trans. II* (1993) 521–523.
- [74] C.A. Tsipis, P.A. Karipidis, Mechanistic Insights into the Bazarov synthesis of urea from NH₃ and CO₂ using electronic structure calculation methods, *J. Phys. Chem. A* 109 (2005) 8560–8567.
- [75] B. Arstad, R. Blom, O. Swang, CO₂ absorption in aqueous solutions of alkanolamines: mechanistic insight from quantum chemical calculations, *J. Phys. Chem. A* 111 (2007) 1222–1228.
- [76] J.A. Tossell, Can two (Environmental) wrongs make a right? The reaction of anthropogenic waste CO₂ and NH₃ to form NH₂COOH, *Environ. Prog. Sustain. Energy* 30 (2011) 692–695.